HIGHWAY RESEARCH RECORD

Number 429

Soils: Loess, Suction, and Frost Action

7 reports
prepared for the
52nd Annual Meeting

Subject Areas

61 Exploration-Classification (Soils)
62 Foundations (Soils)
64 Soil Science

HIGHWAY RESEARCH BOARD
DIVISION OF ENGINEERING NATIONAL RESEARCH COUNCIL
NATIONAL ACADEMY OF SCIENCES—NATIONAL ACADEMY OF ENGINEERING
Washington, D.C. 1973

NOTICE

The studies reported herein were not undertaken under the aegis of the National Academy of Sciences or the National Research Council. The papers report research work of the authors that was done at the institutions named by the authors. The papers were offered to the Highway Research Board of the National Research Council for publication and are published here in the interest of the dissemination of information from research, one of the major functions of the Highway Research Board.

Before publication, each paper was reviewed by members of the HRB committee named as its sponsor and accepted as objective, useful, and suitable for publication by the National Research Council. The members of the review committee were chosen for recognized scholarly competence and with due consideration for the balance of disciplines appropriate to the subject concerned.

Responsibility for the publication of these reports rests with the sponsoring committee. However, the opinions and conclusions expressed in the reports are those of the individual authors and not necessarily those of the sponsoring committee, the Highway Research Board, or the National Research Council.

Each report is reviewed and processed according to the procedures established and monitored by the Report Review Committee of the National Academy of Sciences. Distribution of the report is approved by the President of the Academy upon satisfactory completion of the review process.

ISBN 0-309-02158-8
Library of Congress Catalog Card No. 73-7059
Price: $2.20
Available from
Highway Research Board
National Academy of Sciences
2101 Constitution Avenue, N. W.
Washington, D. C. 20418

CONTENTS

FOREWORD

The broad coverage of soil subjects in this RECORD indicates the breadth of information that a competent soils engineer must cover to stay abreast of the field. All of the extensions of knowledge gleaned here have application in improving the effectiveness of the engineer in making practical applications of his knowledge.

The mechanistic behavior of soils in response to applied loads is dependent on soil particle arrangement and spacing. The papers by Huang and Demirel and by Badger and Lohnes present information on techniques for determining the soil structure of friable loess and quantifying that structure.

As compacted moistures below optimum, lateral swelling pressures were found to be as high as vertical swelling pressures for the 2 cohesive soils studied by Snethen and Haliburton. Recognition of that potential should lead to better construction specifications and construction control, which could do much to alleviate the problem. In his study of soil moisture suctions, Shackel shows how saturation, dry density, and stress history affect the soil suction characteristics. The extension of those findings to field conditions should lead to an overall improvement in the understanding of the performance of soil embankments.

A large portion of this nation contains some soils that have potentially damaging reactions to frost penetration when used as roadbed supports. Efforts to overcome the problem of frost damage have historically taken 2 approaches: identify and remove the offending material or construct in such a way that the penetration of frost to the susceptible material is prevented. Jessberger presents a survey of criteria used to identify frost-susceptible materials. Identification is necessary whether the materials are to be removed or covered. Horton, Bowers, and Lovell present a technical report on a thermally insulated test road. The performance has been satisfactory during the 3 years it has been in service. Limited information on differential surface icing of adjacent insulated and uninsulated sections is also presented. Walsh presents a description of the temperature instrumentation for that same test road. The description will be beneficial to anyone interested in making a similar study.

This RECORD will be of interest to construction, research, and soils engineers.

MICRO-PORE-SIZE ANALYSIS OF A FRIABLE LOESS

Rodney J. Huang, University of California, Berkeley; and
Turgut Demirel, Iowa State University

The sorption isotherm method was used to determine the pore-size distribution of a friable Iowa loess. Both the adsorption and the desorption branches were used for pore-size distribution analysis. The difference between the 2 branches was interpreted as an indication of the extent of constrictions within the pore structure according to McBain's "ink-bottle" theory. Pore-size distribution curves obtained from the adsorption isotherm were compatible with mercury porosimetry results. Procedures for evaluation of pore-size distribution from sorption data are described, and the pore-size range is noted.

THE TOTAL specific surface area of a porous solid, the distribution of total surface area, and the pore-volume distribution as a function of pore sizes have become progressively more important in understanding chemical and physical behavior of porous materials. Those characteristics have long been recognized as important, for example, in the assessment of the chemical activity of catalysts.

Soil structure has long been recognized as important in the field of soil mechanics. Significant advances have been made toward its determination and toward understanding its effect on the mechanistic behavior of soils (1, 2), but the first significant approach to the problem through pore-size distribution has been made rather recently by Diamond and his coworkers (3, 4).

Two independent methods exist for pore-size distribution analysis. The first, the mercury-injection method, was suggested by Washburn in 1921 (5) and was later fully developed by Ritter and Drake (6). The second, the isotherm method, was proposed by Wheeler in 1945 and was further developed by him and others (7, 8, 9, 10, 11, 12). In an extensive investigation undertaken at Iowa State University to correlate the engineering behavior of soils with soil structure (13), both of those techniques were used. The results of the mercury-injection method on disturbed and undisturbed samples of a friable Iowa loess are reported by Badger and Lohnes (14). The isotherm method was used only for the undisturbed loess sample, and the results obtained are presented, analyzed, and compared with the results of mercury-injection method in this paper.

SORPTION ISOTHERM METHOD FOR PORE-SIZE DISTRIBUTION ANALYSIS

Analysis of sorption isotherms has been extensively used to study the pore structure of various materials. Most of the methods developed during the past 25 years make use of Kelvin's capillary condensation equation and Brunauer, Emmett, and Teller's multilayer adsorption theory (15). The starting point of those methods is the equation proposed by Wheeler in 1946 (7, 8, 10). The first method to enjoy a universal acceptance was developed by Barrett, Joyner, and Halenda in 1951 (10) and is now known as the BJH method. The methods developed since then, such as those of Cranston and Inkley (12) and Pierce (11), have been revisions of the BJH method. There are other commonalities of those methods:

1. The use of nitrogen gas as the adsorbate;

Sponsored by Committee on Physicochemical Phenomena in Soils.

2. The assumption that the Kelvin radius of capillary condensation is equal to the pore radius minus the thickness of the adsorbed film; and

3. The evaluation of the adsorbed film thickness from nitrogen adsorption isotherms on nonporous adsorbents (t-curves—sorption isotherm depicted by film thickness versus relative pressure), which impose on the flexibility of the method and on the interpretation of the results the restrictions of (a) adsorbate limited to nitrogen, (b) pore shapes assumed to be cylindrical, and (c) a somewhat arbitrary film thickness (t-curves) because all data used for those methods are obtained from other so-called representative nonporous adsorbents.

Recently Brunauer and coworkers (16, 17, 18, 19, 20, 21) published a series of papers leading to the development of new methods for micro- and macro-pore-size distribution analyses. They have replaced the Kelvin radius with hydraulic radius (16) and based the adsorbed film thickness on the value of the BET parameter C (18, 21). That broadens the physical meaning of pore-size distribution analyses and eliminates most of the uncertainties from the evaluation of adsorbed film thickness.

However, for consistency with mercury porosimetry data, the pore-size distribution in the present paper is expressed in terms of Kelvin radii rather than hydraulic radii. The adsorbed film thicknesses were taken from Brunauer et al. (21) on the basis of BET parameter C. The method of analysis used is that of Pierce (11) offered in 1953. The Pierce method was selected because of its simplicity and clarity in spite of its unpopularity. An outline of the method is given below.

The vapor pressure p of a liquid adsorbate condensed in a capillary of radius r_k (Kelvin radius) and in equilibrium with its vapor is given by the following Kelvin equation if the capillary is completely wettable by the adsorbate:

$$\ln p/p_o = \frac{-2\,\gamma\,\overline{V}}{RT\,r_k} \tag{1}$$

where p_o is the saturation vapor pressure of the adsorbate, γ is its surface tension, and $\overline{V}$ is the molar volume of the adsorbate. If the vapor pressure of adsorbate over a porous adsorbent is increased to a value given by Eq. 1, the closed-end pores having radii equal to or smaller than r_k will be completely filled by capillary condensation. For the reverse process (i.e., if the vapor pressure is decreased to a given p/p_o value), completely filled pores having radii equal to or larger than r_k of Eq. 1 will empty. The equivalent pore radius r_p is calculated by Eq. 2 where r_k is an equivalent pore radius and t is the thickness of the film adsorbed on the surfaces of capillaries at any given p/p_o.

$$r_p = r_k + t \tag{2}$$

During an adsorption or desorption isotherm experiment, if the relative pressure is changed from $(p/p_o)_1$ to $(p/p_o)_2$, pores with corresponding Kelvin radii between r_{k1} and r_{k2} (Eq. 1) will either fill or empty depending on the sorption branch being adsorbed or desorbed respectively. That is accompanied by a change ΔV in the total volume of adsorbate V adsorbed by the porous adsorbent. Part of the change ΔV is due to adsorption or desportion of the adsorbate from the free surface as expressed below:

$$\Delta V = \Delta V_k + \Delta V_f \tag{3}$$

where ΔV_k is the volume adsorbed or desorbed because of capillary condensation (inner capillary or core volume) and ΔV_f is the volume of the adsorbate that is adsorbed or desorbed from the free surfaces and that results in a change of the thickness of the adsorbed film from t_1 to t_2 on free surfaces. The thickness t can be expressed in terms of the number of molecular layers n as follows:

$$t = n \cdot \delta \tag{4}$$

where δ is the thickness of one adsorbate molecule.

The volume ΔV_k is the volume of capillaries having radii from r_{k1} to r_{k2} exclusive of assumed adsorbed film in those capillaries, which is referred to as inner-capillary volume (11) or pore volume (16). Then, the net volume of capillaries ΔV_p, filled or emptied in this range, is expressed as

$$\Delta V_p = R_r \Delta V_k \tag{5}$$

where

$$R_r = (r_p/r_k)^2 \tag{6}$$

The adsorbate volume ΔV_f, desorbed from or adsorbed on the free surface for each p/p_o increment, is expressed as follows:

$$\Delta V_f = \Delta n \cdot \delta \cdot \Sigma A_p \tag{7}$$

where Δn is the number of the monomolecular layers adsorbed or desorbed from free surface, δ is the thickness of one molecule of the adsorbate, and A_p is the area of the empty pores or free surface. The latter is expressed as follows:

$$A_p = 2\Delta V_p/\bar{r}_p \tag{8}$$

where $\bar{r}_p$ is the average pore radius for the average relative vapor pressure $(\bar{p}/\bar{p}_o)$, as expressed in Eqs. 9 and 10.

$$\bar{r}_p = \frac{r_{p1} + r_{p2}}{2} \tag{9}$$

$$(\bar{p}/\bar{p}_o) = \frac{(p/p_o)_1 + (p/p_o)_2}{2} \tag{10}$$

After those relationships are established, the Pierce method proceeds with a set of calculations from sorption isotherms starting with $p/p_o = 1$ and t-curves leading to pore-size distribution, which is summarized in the steps below as it is used in the present paper with minor modifications.

1. p/p_o versus V is obtained from sorption isotherms.
2. n and t values are obtained from established t-curves for each p/p_o on the basis of BET parameter C, which is obtained from the BET plot of the sorption isotherm.
3. r_k values corresponding to each p/p_o are calculated from Eq. 1.
4. r_p values corresponding to each p/p_o are calculated from Eq. 2 and step 2.
5. R_r values are calculated from Eq. 6.
6. $\bar{r}_p$ values are calculated from Eq. 9 and step 4, the corresponding $(\bar{p}/\bar{p}_o)$ values are calculated from Eq. 10, and then $1/\bar{r}_p$ is plotted versus log $\bar{p}/\bar{p}_o$.
7. Δn values for each p/p_o increment are calculated from step 2.
8. ΔV values for each p/p_o increment are calculated from step 1.

a. ΔV_k value for the first sorption increment to $p/p_o = 1$ (if the adsorption branch is used) or from $p/p_o = 1$ (if the desorption branch is used) is determined from step 1. Because there is no free surface on a porous adsorbent at $p/p_o = 1$, i.e., all the pores are filled up by capillary condensation, $\Delta V_k = \Delta V$ and $\Delta V_f = 0$.

b. ΔV_p value for the first sorption increment is calculated from Eq. 5 and steps 5 and 8a.

c. $\bar{r}_p$ value for the first sorption increment is determined from the plot of step 6 by extrapolation.

d. A_p value for the first sorption increment is calculated from Eq. 8 and steps 8b and 8c. That value of A_p is to be used for the next sorption increment.

Results obtained in steps 6 and 8b constitute the coordinates of the first point of the pore-size distribution curve. The subsequent points are determined by the use of steps 1 to 8 and steps 9 to 14 given below:

9. ΔV_f values are calculated from Eq. 7 and steps 7 and 8d for the second sorption increment and from Eq. 7 and steps 7 and 14 for the subsequent sorption increments.
10. ΔV_k values are calculated from Eq. 3 and steps 8 and 9.
11. ΔV_p values are calculated from Eq. 5 and steps 5 and 10.
12. A_p values are calculated from Eq. 8 and steps 11 and 6.
13. $\Sigma\Delta V_p$ values are calculated from the results of step 11 (the summation is carried out from lowest p/p_o to $p/p_o = 1$).
14. ΣA_p values are calculated from the results of step 12.

Results obtained in steps 6 and 11 constitute the coordinates of pore-size distribution curves.

The original Pierce method (11) was developed for desorption isotherms of nitrogen. The t-curve data for nitrogen available to Pierce at that time were too high as reported by him later (22). The ambiguity of t-curve data that we believed existed all along has recently been eliminated by Brunauer and his coworkers (18, 21) enabling researchers to use not only nitrogen but other adsorbates. In the present work, water vapor was used as the adsorbate on the basis of the data of Brunauer et al. (21). Choice of water was made for 2 reasons: First, not all pores and surfaces of soil minerals are accessible to nitrogen, whereas they are to water vapor (21, 23, 24, 25); and, second, use of water vapor as adsorbate simplifies the experimental procedure. Other minor revisions of the Pierce method made in the present paper are use of both adsorption and desorption data for reasons to be explained later and determination of $\bar{r}_p$ for the first sorption increment from $p/p_o = 1$ as explained above in step 8c. Pierce (11) offers no explanation of how $\bar{r}_p$ for the first increment is obtained.

EXPERIMENTAL ANALYSIS

Instrumentation

The sorption isotherms were determined gravimetrically by the use of a Cahn RG electrobalance coupled with an automatic Sargent recorder. The sample weight was determined to microgram sensitivity. The instrument was calibrated prior to the test, and a buoyancy correction was applied. Room temperature was maintained at 22 ± 0.25 C throughout the investigation.

A capacitance manometer was used to prevent mercury contamination and to maintain a pure adsorbent-adsorbate system. It operated as a null indicator for the system. The true pressure was read from a mercury manometer with a vernier micrometer slide cathotometer. The pressures are accurate to 1 μm of mercury.

A rotary mechanical fore pump and an oil diffusion pump provided a vacuum of 10^{-6} torr. The sample was suspended from an arm of the microbalance into a glass hang-down tube immersed in a constant temperature bath maintained at 20.00 ± 0.01 C. Temperature readings were taken with a Beckman thermometer, accurate to ± 0.002 C. The Beckman thermometer was calibrated against a thermometer, certified by the National Bureau of Standards, at the thermostat temperature. The detailed description of the system is given elsewhere (26, 27).

Experimental Procedure

The sample in the system was evacuated for 2 weeks at a room temperature of 22 C. The hang-down tube containing the sample and all parts of the adsorption system except the microbalance were heated for 12 hours to about 300 C. The sample was heated occasionally during degassing with an infrared heater. The water in the reservoir was also degassed during the period of evacuation after it was frozen in liquid nitrogen; that was done at least 5 times until no dissolved air was left. When the system reached 10^{-6} torr (determined with a calibrated discharge gauge), the pumping valve was closed for 2 hours to determine whether degassing was complete. The part of the system con-

nected to the capacitance manometer was also pumped down at the same time. Finally, the system was sealed, and the capacitance manometer was calibrated.

Water vapor was transferred into the system from the water reservoir in the range of $p/p_o = 0$ to $p/p_o = 1$. The amount of water adsorbed on the sample was automatically registered on the recorder, and the water vapor pressure was determined. System equilibrium was attained when there was no increase in sample weight and no drop of system pressure. A 24-hour period was allowed to ensure that equilibrium had occurred.

The desorption isotherms were obtained by condensing more and more vapor back into the water reservoir. That condensation process was performed by cooling the water reservoir first with an ice-water mixture and then with a dewar flask containing liquid nitrogen.

Materials Used

The soil sample used in the present study was an undisturbed hand-carved friable Iowa loess obtained from Prospect Hill in Sioux City, Iowa. Its engineering properties are given in Table 1. Its dry density and porosity were determined from bulk dimensions and oven-dry weight of hand-carved specimens.

RESULTS AND DATA ANALYSIS

The water sorption isotherms of the undisturbed loess sample at 20 C exhibit a strong hysteresis (Fig. 1). BET plots of sorption data are shown in Figure 2. The BET parameters V_m and C calculated from Figure 2 are 0.0135 cm^3/g and 20 for the adsorption branch and 0.0180 cm^3/g and 54.7 for the desorption branch respectively. The total specific surface of the sample calculated from the BET parameter V_m is 48.7 m^2/g from the adsorption isotherm and 64.8 m^2/g from the desorption isotherm. The specific surface calculated from the desorption isotherm is about 33 percent higher than that calculated from the adsorption isotherm.

Pore-size distribution data are given in Tables 2 and 3 for adsorption and desorption respectively. Data are compiled in those tables in accordance with the 14-step procedure described earlier. The statistical number of layers n are obtained from Hagymassy, Brunauer, and Mikhail (21). A plot of $\log \bar{p}/\bar{p}_o$ versus $1/\bar{r}_p$ is shown in Figure 3, which was used to obtain $\bar{r}_p$ value for the first sorption increments from $p/p_o = 1$.

Hysteresis Loop

The identification of the true equilibrium branch of sorption isotherms of porous solids has been a subject of argument for more than half a century (24, 17). Those rejecting the adsorption branch base their arguments on either Zsigmondy's explanation of incomplete wetting during adsorption due to impurities or on Foster's explanation of delayed nucleation of menisci in open-ended capillaries in the range of capillary condensation during the adsorption process. Those rejecting the desorption branch base their arguments on McBain's explanation of delayed desorption of the adsorbate trapped in pores with narrow necks shaped like ink bottles. Although each constitutes a partial explanation, together they constitute a reasonable explanation of sorption hysteresis in general. The Zsigmondy explanation gives rise to a diagnostic irreversible hysteresis and can be eliminated by drastic evacuation, whereas the Foster and McBain explanations cause permanent reversible hysteresis. The latter two types, however, if coexisting, defy the existence of an equilibrium branch.

In making a choice, therefore, one must examine the system by assessing to what extent each of those types may be effective and if one of them may be considered negligible. Such an examination has been presented by Brunauer et al. (17). It led them to use the adsorption branch for pore-structure analysis of hardened portland cement pastes; however, the desorption branch has found large-scale acceptance in the literature. In the present work the adsorption isotherm has been used as the branch closest to equilibrium. Zsigmondy hysteresis is believed to be minimized by the drastic evacuation. The choice, then, between Foster and McBain was made on the basis of the

Figure 1. Sorption isotherms of water vapor on friable loess.

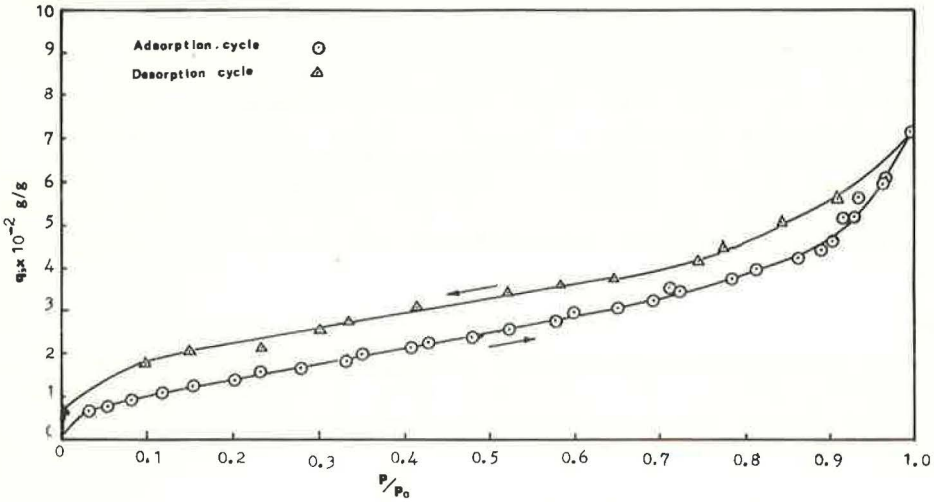

Table 1. Properties of friable Iowa loess.

Property	Amount
Specific gravity	2.7[a]
Undisturbed dry density, lb/ft^3	85.3
Undisturbed porosity, percent	49.4
Undisturbed void ratio, cm^3/cm^3	0.975
Undisturbed void volume, cm^3/g	0.361
Liquid limit, percent	30
Plastic limit, percent	26
Standard Proctor compaction	
Optimum moisture, percent	16.5
Maximum dry density, lb/ft^3	109.4
Grain-size distribution, percent	
Clay (< 2 μm)	14
Silt (2 to 74 μm)	86
AASHO classification	A-4(8)
Field moisture, percent	7 to 10
Strength parameters	
Internal friction angle, deg	32.2
Cohesion, lb/in.^{2}	1.0
Minerals present (X-ray analysis)	Quartz, montmorillonite illite, calcium carbonate, dolomite, and feldspar

[a]Average of 9 tests.

Figure 2. BET for water vapor on friable loess.

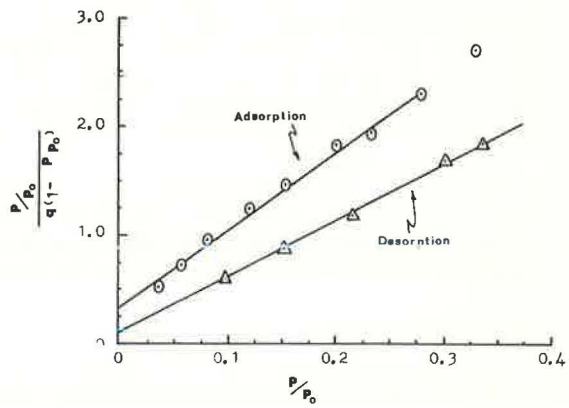

Table 2. Pore-size distribution analysis of undisturbed loess sample—adsorption.

Step	Parameter	Values for Each Increment														
1	p/p_o	1.000	0.963	0.926	0.901	0.862	0.812	0.682	0.597	0.479	0.407	0.333	0.234	0.155	0.083	0
	V, cm^3/g	0.0713	0.0607	0.0518	0.0464	0.0426	0.0395	0.0327	0.0297	0.0240	0.0213	0.0184	0.0157	0.0127	0.0094	0
2	n	6.05	4.45	3.85	3.56	3.17	2.80	2.30	1.98	1.75	1.57	1.41	1.17	0.95	0.72	0
	t, Å	18.15	13.35	11.55	10.68	9.51	8.40	6.90	5.94	5.25	4.71	4.23	3.51	2.85	2.16	0
3	r_k, Å		0.270	140	1.05	73	51	28	20	12.5	11.0	9.5	7.5	5.8	4	0
4	r_p, Å		283.35	151.55	115.68	82.51	59.40	34.90	25.94	17.75	15.71	13.73	11.01	8.65	6.16	
5	$\frac{R_r}{}$		1.10	1.17	1.21	1.28	1.35	1.55	1.67	2.01	2.04	2.08	2.14	2.25	2.36	
6	$\frac{p/p_o}{\bar{r}_p}$, Å	0.979 (625)[a]	0.944 217.45	0.913 133.61	0.881 99.09	0.837 70.95	0.752 47.65	0.644 30.42	0.538 21.84	0.443 16.73	0.370 14.97	0.283 12.37	0.194 9.83	0.119 7.40	0.041 3.08	
7	Δn	1.41	0.60	0.29	0.39	0.37	0.50	0.32	0.23	0.18	0.16	0.24	0.22	0.23	0.72	
8	ΔV, cm^3/g	0.0106	0.0089	0.0054	0.0038	0.0031	0.0068	0.0030	0.0057	0.0027	0.0029	0.0027	0.0030	0.0033	0.0094	
9	ΔV_t, cm^3/g	0	0.0001	0.0001	0.0002	0.0003	0.0006	0.0008	0.0007	0.0010	0.0011	0.0020	0.0020	0.0024	0.0089	
10	ΔV_k, cm^3/g	0.0106	0.0088	0.0053	0.0035	0.0027	0.0061	0.0022	0.0050	0.0016	0.0018	0.0007	0.0010	0.0009	0.0005	
11	ΔV_p, cm^3/g	0.0116	0.0103	0.0064	0.0045	0.0037	0.0095	0.0036	0.0100	0.0033	0.0037	0.0015	0.0022	0.0021	0.0020[b]	
12	A_p, m^2/g	0.37	0.95	0.96	0.91	1.05	4.00	2.41	9.20	3.97	5.00	2.42	4.58	5.68	7.16[b]	
13	$\Sigma\Delta V_p$, cm^3/g	0.0744	0.0628	0.0525	0.0461	0.0416	0.0379	0.0284	0.0246	0.0148	0.0115	0.0078	0.0063	0.0041	0.0020	
14	ΣA_p, m^2/g	0.37	1.32	2.28	3.19	4.24	8.24	10.65	19.85	23.82	28.82	31.24	35.82	41.51	48.67[b]	

[a]Obtained from Figure 3.

[b]Based on the total BET specific surface area of 48.67 m^2/g as follows: $A_p = 48.67 - 41.51 = 7.16$ m^2/g; and $\Delta V_p = \Delta V_k + \Delta n \times \delta \times A_p = 0.005 + 0.72 \times 3 \times 10^{-4} \times 7.16 = 0.0020$ cm^3/g.

following argument: In consolidated fine-particulate systems, such as clayey soils, particle-to-particle contacts are believed to be intimate enough to furnish the seat for meniscus nucleation through multilayer adsorption in the early stages of adsorption, eliminating most of the open-ended pores and producing an ink-bottle type of pore. Persistence of the hysteresis to the origin supports that assumption.

Pore-Surface and Pore-Volume Distributions

The values of A_p calculated from adsorption and desorption isotherms are shown in Figure 4. Data shown in Figure 4 and given in Tables 2 and 3 reveal that (a) about 80 percent of the total surface area is located in capillaries smaller than 28 Å in radius; and (b) the largest concentration of the surface area is found in small capillaries of 10 and 50 Å in diameter.

Pore-volume distribution curves corresponding to adsorption and desorption isotherms are shown in Figures 5 and 6. Based on the assumption that the adsorption isotherm is the equilibrium branch, curve A shown in Figure 5 or Figure 6 represents the correct pore-size distribution and curve D represents the size distribution of bottle necks on an exaggerated scale, i.e., as if the voids constricted by the bottle necks are all of neck diameter. Thus, the difference between the 2 curves can be taken as an indication of the extent of constrictions in the pore structure.

The pore-size distribution obtained from the adsorption isotherm is combined with the pore-size distribution of the same friable loess sample obtained by mercury injection (13, 14) shown in Figures 7 and 8. The agreement between the lower end of the distribution function curve obtained from the adsorption isotherm (Fig. 7) is quite striking. Also, the smooth transition between the cumulative percentage of pore-volume distribution curves obtained by the 2 methods (Fig. 8) shows that mercury injection and adsorption isotherm methods are compatible. Percentage of cumulative pore volumes was calculated as percentages of the total pore volume 0.361 cm^3/g (Table 1).

DISCUSSION OF RESULTS

The gross results of pore-size distribution analysis are given in Table 4. The combined average pore-diameter range (covered by both the sorption isotherm and the mercury-injection methods) extends from about 6×10^{-4} to 32 μm accounting for about 91 percent of the total void volume determined from bulk properties of the sample (Table 1). The adsorption isotherm method accounts for about 20 percent and mercury injection for about 73 percent of that volume with an overlap in the range of 0.0585 to 0.0625 μm radius covering about 2 percent of the total voids (Fig. 8). The upper limit of average pore radius of 16 μm (32 μm in diameter) corresponds to the volume injected by mercury in the pressure range of 5 to 10 lb/in^2. Because the mercury-injection data in the range of 0 to 1 lb/in^2 were open to question and because the average pore radius in that range is indeterminate, the data corresponding to that range have been excluded from the present paper. The volume of the pores having diameters larger than 32 μm was then found to be about 9 percent after the curves of the 2 methods were superimposed as shown in Figure 8.

Comparison of the specific surface areas obtained from pore-size analysis with those obtained from BET plots has been a generally accepted criterion for assessment of the dependability of the pore analysis. Another criterion is the comparison of the total volume determined from pore analysis with that directly determined from sorption isotherms. Those criteria have been criticized by Brunauer (18). The pore-size analysis can only be as accurate as the BET analysis and as the total volume of adsorbate determined at $p/p_o = 1$. Any large deviation beyond those due to the pore-shape considerations and experimental error should be attributable to the assumed boundaries, i.e., the upper and the lower ends of the p/p_o range covering the capillary condensation. For example, if the lower boundary of p/p_o was taken as 0.333 (Table 2), the total surface area ΣA_p would have a value of 28.82 m^2/g and the total pore volume $\Sigma \Delta V_p$ would be 0.0103 cm^3/g as compared to the BET area of 48.67 m^2/g and the total pore volume of 0.0713 cm^3/g.

Table 3. Pore-size distribution analysis of undisturbed loess sample—desorption.

Step	Parameter	Values for Each Increment														
1	p/p_o	1.0	0.909	0.842	0.772	0.745	0.661	0.582	0.518	0.411	0.336	0.304	0.216	0.153	0.097	0
	V, cm^3/g	0.0713	0.0555	0.0508	0.0449	0.0413	0.0387	0.0376	0.0360	0.0341	0.0306	0.0277	0.0232	0.0205	0.0179	0.0063
2	n	6.06	3.65	3.05	2.60	2.48	2.20	2.15	1.96	1.72	1.60	1.45	1.26	1.17	1.03	
	t, Å	18.18	10.95	9.15	7.80	7.44	6.60	6.45	5.88	5.16	4.80	4.35	3.78	3.51	2.09	
3	r_k, Å		115	62	40	35	25	23	19	15	11.5	10.0	7.3	6.0	4.8	0
4	r_p, Å		125.95	71.15	47.80	42.44	31.60	29.45	24.88	20.16	16.30	14.35	11.08	9.51	7.89	
5	R_r	1.00	1.20	1.31	1.42	1.47	1.59	1.64	1.72	1.80	2.00	2.06	2.30	2.51	2.70	
6	$\overline{p/p_o}$	0.954	0.875	0.807	0.758	0.703	0.621	0.550	0.464	0.373	0.320	0.260	0.184	0.125	0.048	
	$\overline{r}_p$, Å	(312)[a]	98.55	59.47	45.12	37.02	30.52	22.52	18.23	15.32	13.77	12.14	10.29	8.70	3.95	
7	Δn	2.41	0.60	0.35	0.12	0.28	0.05	0.24	0.24	0.12	0.15	0.19	0.09	0.14	1.03	
8	ΔV, cm^3/g	0.0158	0.0047	0.0059	0.0036	0.0026	0.0011	0.0016	0.0019	0.0035	0.0029	0.0045	0.0027	0.0026	0.0116	
9	ΔV_r, cm^3/g	0	0.0002	0.0003	0.0002	0.0006	0.0001	0.0007	0.0008	0.0005	0.0009	0.0015	0.0010	0.0020	0.0104	
10	ΔV_k, cm^3/g	0.0158	0.0045	0.0056	0.0034	0.0020	0.0010	0.0009	0.0011	0.0030	0.0020	0.0030	0.0017	0.0006	0.0012	
11	ΔV_p, cm^3/g	0.0189	0.0059	0.0079	0.0050	0.0032	0.0016	0.0016	0.0020	0.0060	0.0041	0.0069	0.0043	0.0016	0.0054[b]	
12	A_p, m^2/g	1.21	1.20	2.70	2.23	1.72	1.07	1.37	2.19	7.83	5.96	11.38	6.54	3.68	13.72	
13	$\Sigma\Delta V_p$, cm^3/g	0.0744	0.0555	0.0496	0.0417	0.0367	0.0335	0.0319	0.0303	0.0283	0.0223	0.0182	0.0113	0.0070	0.0054	
14	ΣA_p, m^2/g	1.21	2.41	5.11	7.34	9.06	10.13	11.50	13.69	21.52	27.48	38.86	47.40	51.08	64.80[b]	

[a] Obtained from Figure 3.
[b] Based on the total BET specific surface area of 64.80 as follows: $A_p = 64.80 - 51.08 = 13.72\ m^2/g$; and $\Delta V_p = \Delta V_k + \Delta n \times \delta \times A_p = 0.0012 + 1.03 \times 3 \times 10^{-4} \times 13.72 = 0.0054\ cm^3/g$.

Figure 3. p/p_o versus $1/\overline{r}_p$.

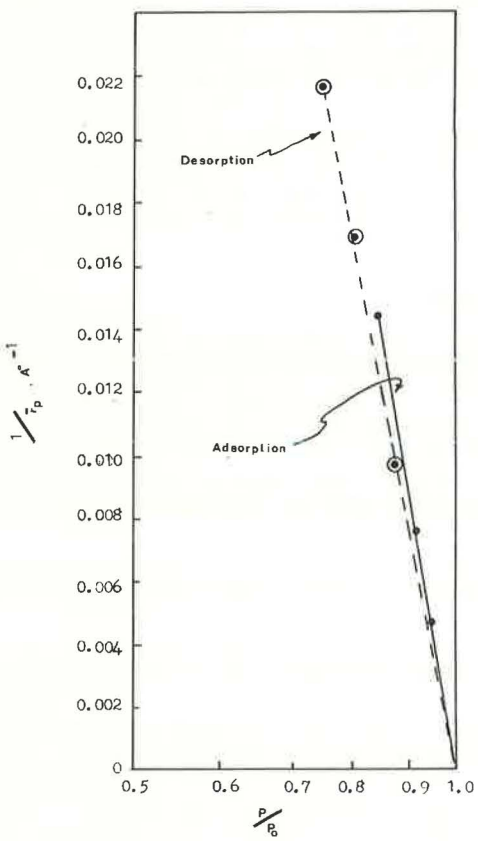

Figure 4. Surface-area distribution of friable loess.

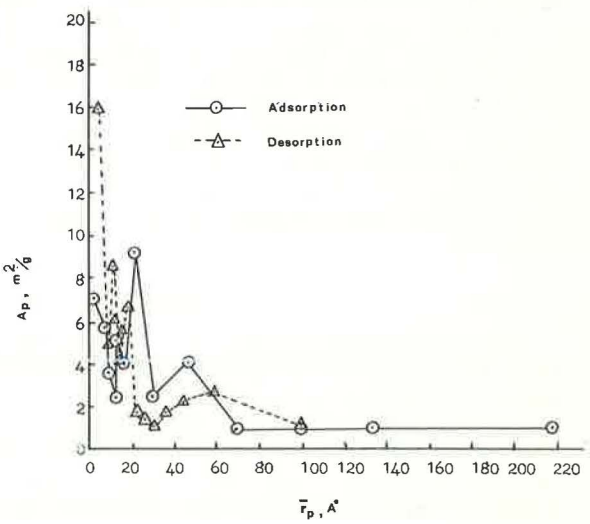

Figure 5. Pore-volume distribution of friable loess.

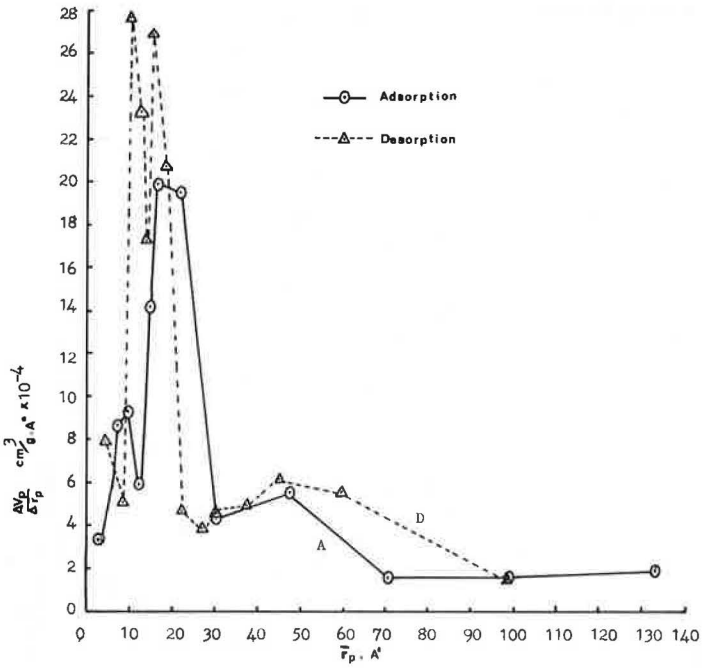

Figure 6. Cumulative pore-volume distribution of friable loess.

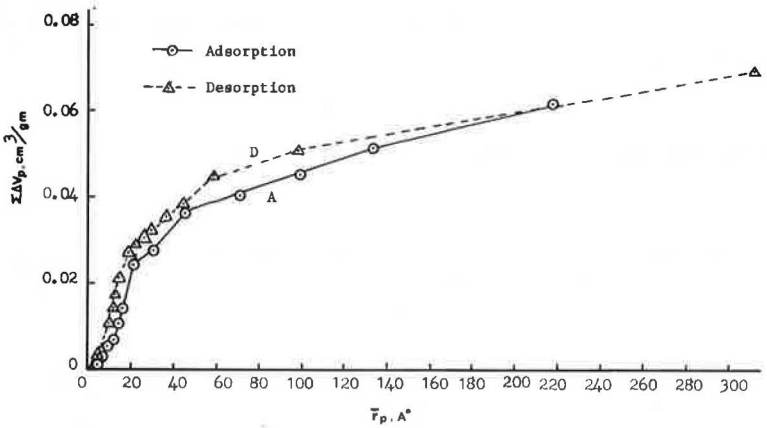

Table 4. Summary of pore-size analysis of friable Iowa loess.

Method	$\Sigma\Delta V_p$ (cm^3/g)	Specific Surface Area (m^2/g)	Average Pore Radius (μm) Lower Limit	Upper Limit	$\frac{\Sigma\Delta V_p}{V_t}$
Sorption isotherm pore analysis					
Adsorption	0.0744	48.7*	3.1×10^{-4}	0.063	0.203
Desorption	0.0744	64.8*	4.0×10^{-4}	0.0312	0.203
Mercury injection pore analysis	0.265		0.058	16.0	0.734
Sorption isotherm and BET analysis					
Adsorption	0.0713	48.7			0.198
Desorption	0.0713	64.8			0.198
Bulk properties	0.361				1.00

Note: $\Sigma\Delta V_p$ is the total pore volume, and V_t is the total pore volume determined from bulk properties.

*Assumed to be equal to BET specific surface area as a necessary condition.

Figure 7. Combined pore-volume distribution of friable loess.

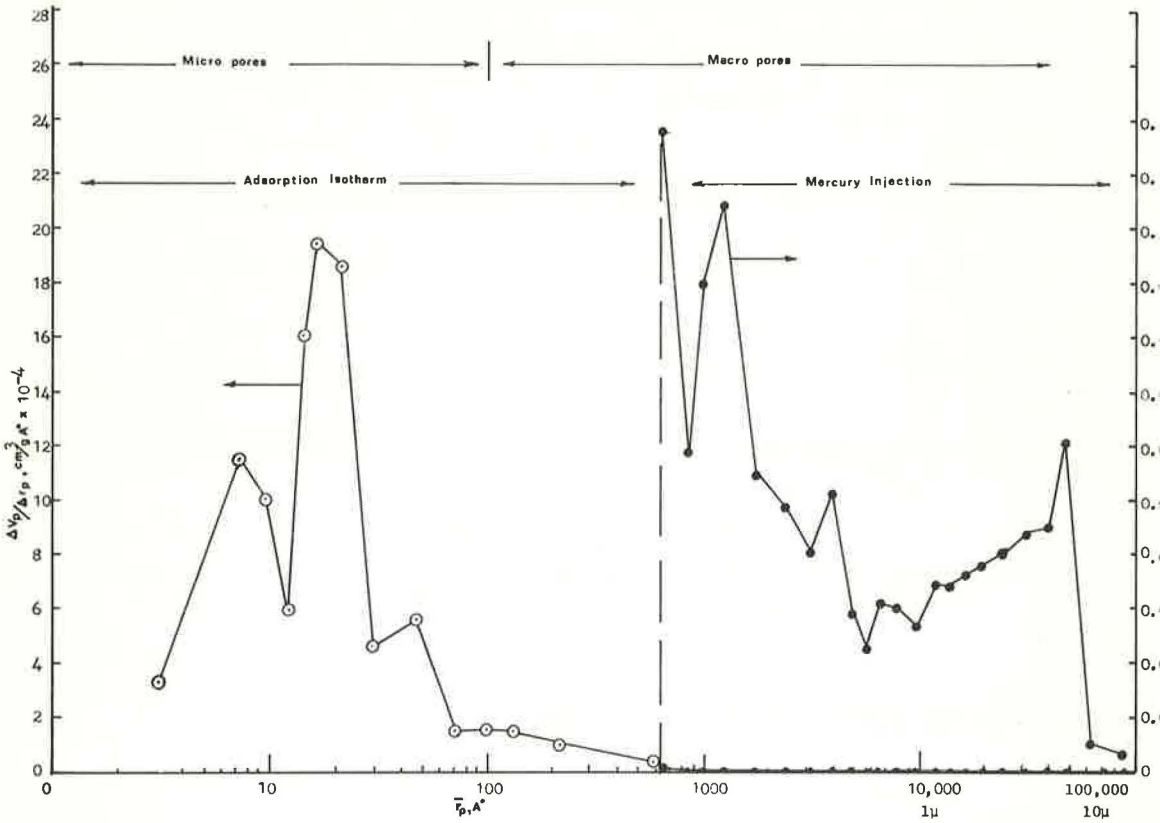

Figure 8. Normalized cumulative pore-volume curve of friable loess.

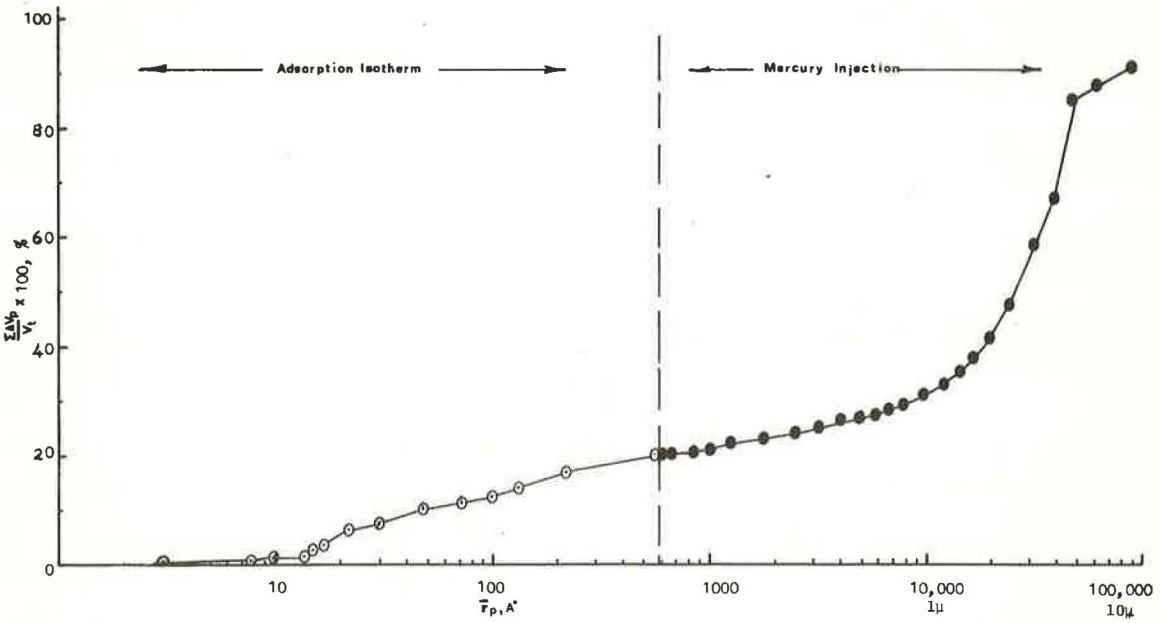

Normally pore-size analysis is carried to the point where the hysteresis loop is closed on the assumption that the hysteresis loop covers the range of all pore sizes. But an agreement between the results of pore analysis and BET specific surface area, i.e., total pore volume, is not always obtained, and seldom are significant differences between the 2 results observed. According to Brunauer et al. (18), that difference can be attributed to micropores smaller than 15 Å in diameter, which fill by multilayer adsorption. In the present paper, total specific surface and total pore volume agreements are used as a necessary condition to be fulfilled, and the last p/p_o increment was chosen so that this criterion is met. To do that, the calculation procedure for the last p/p_o increment (last column of Table 2 or Table 3) was modified and the incremental area A_p was calculated as a difference between BET specific surface and total pore area calculated to the last increment, $A_{BET} - \Sigma A_p$.

From the sorption isotherm, the total volume of pores filled at saturation relative pressure ($p/p_o = 1$) is 0.0713 cm^3/g, which is about 20 percent of the total pore volume of 0.361 cm^3/g determined from bulk properties. Evidently very large pores do not fill by capillary condensation, either because of slow condensation rates or more likely because large open-ended pores with plane surfaces inhibit nucleation of menisci.

The loess used contained 14 percent of clay sizes in which unknown amounts of expansive montmorillonite were present (Table 1). The expansive characteristics of expanding 3-layer clays such as montmorillonite may be a damaging factor in pore-size distribution analysis in which water vapor is used as an adsorbate. However, from the pore-size distribution curves and the cumulative pore-volume curve of friable loess used, the authors found no evidence of expansion. It is suggested that use of water vapor and void-expanding-inert vapors, i.e., nitrogen, as adsorbate may be extremely essential in distinguishing the expansive extension of the soils under investigation. Further research is needed in applying the modified Pierce's method in conjunction with mercury-injection porosimetry to various nonexpansive and expansive soils.

SUMMARY AND CONCLUSIONS

A method using sorption isotherm data to analyze pore-size distribution is presented. The method, combined with a mercury porosimetry technique, indicates that pore-size distribution can be determined. The main findings of this investigation are summarized below.

1. The Pierce method was modified and advanced to determine pore-size distribution of a friable Iowa loess using water-sorption isotherm data. The method can be used for different adsorbates on different soil materials.
2. Both adsorption and desorption branches were used for pore-size distribution analysis. The difference between the 2 branches was interpreted as an indication of the extent of constrictions within the pore structure according to McBain's ink-bottle theory.
3. Pore-size distribution curves obtained from the adsorption isotherm were compatible with mercury porosimetry results. Practically, the adsorption isotherm method covers the pores from 0 to 600 Å in radius, and the mercury-injection method covers the rest of the bigger pores.
4. The pore-size distribution of soil may be significant in the analysis of soil structure in relation to permeability, cohesion, and surface activity of the soil matter.

ACKNOWLEDGMENTS

The authors gratefully acknowledge the support given by the Environmental Sciences Division, Army Research Office, Durham, North Carolina. The authors would also like to acknowledge the sponsorship of the Engineering Research Institute at Iowa State University. The senior author acknowledges NASA for the partial financial support from the National Aeronautics and Space Administration.

REFERENCES

1. Mitchell, J. K. The Fabric of Natural Clays and Its Relation to Engineering Properties. HRB Proc., Vol. 35, 1956, pp. 693-713.
2. Skempton, A. W. Long-Term Stability of Clay Slopes. Geotechnique, Vol. 14, 1964, pp. 75-102.
3. Diamond, S. Pore-Size Distribution in Clays. Clays and Clay Miner., Vol. 13, No. 1, 1970, pp. 7-23.
4. Sridharan, A., Altschaeffl, A. G., and Diamond, S. Pore Size Distribution Studies. J. Soil Mech. and Found. Div., Proc. ASCE., Vol. 97 No. SM5, 1971, pp. 771-787.
5. Washburn, E. W. Note on a Method of Determining the Distribution of Pore Sizes in a Porous Material. Nat. Acad. Sci. Proc, Vol. 7, 1921, pp. 115-116.
6. Ritter, H. L., and Drake, L. C. Pore-Size Distribution in Porous Materials; Pressure Porosimeter and Determinations of Complete Macropore-Size Distribution. Ind. Eng. Chem. Anal. Ed., Vol. 17, 1945, pp. 782-786.
7. Wheeler, A. Reaction Rates and Selectivity in Catalyst Pores. Adv. in Catalysis and Relat. Subj., Vol. 3, 1951, pp. 249-327.
8. Wheeler, A. Reaction Rates and Selectivity in Catalyst Pores. Catalysis, Vol. 2, 1955, pp. 105-123.
9. Oulton, T. D. The Pore Size-Surface Area Distribution of a Cracking Catalyst. J. Phys. Chem., Vol. 52, 1948, pp. 1296-1314.
10. Barrett, E. P., Joyner, L. G., and Halenda, P. P. The Determination of Pore Volume and Area Distribution in Porous Substances: I—Computations From Nitrogen Isotherms. J. Am. Chem. Soc., Vol. 73, 1951, pp. 373-380.
11. Pierce, C. Computation of Pore Sizes From Physical Adsorption Data. J. Phys. Chem., Vol. 57, 1953, pp. 149-152.
12. Cranston, R. W., and Inkley, F. A. The Determination of Pore Structures From Nitrogen Adsorption Isotherms. Adv. in Catalysis and Relat. Subj., Vol. 9, 1957, pp. 143-154.
13. Badger, W. W. Structure of Friable Iowa Loess. Library, Iowa State Univ., Ames, PhD thesis, 1972.
14. Badger, W. W., and Lohnes, R. A. Structure of Friable Iowa Loess. Paper presented at HRB 52nd Annual Meeting and published in this Record.
15. Brunauer, S., Emmett, P. H., and Teller, E. Adsorption of Gases in Multimolecular Layers. J. Am. Chem. Soc., Vol. 60, 1938, pp. 309-319.
16. Brunauer, S., Mikhail, R. S., and Bodor, E. E. Pore Structure Analysis Without a Pore Shape Model. J. Colloid and Interf. Sci., Vol. 24, 1967, pp. 451-463.
17. Brunauer, S., Mikhail, R. S., and Bodor, E. E. Some Remarks About Capillary Condensation and Pore Structure Analysis. J. Colloid and Interf. Sci., Vol. 25, 1967, pp. 353-358.
18. Mikhail, R. S., Brunauer, S., and Bodor, E. E. Investigation of a Complete Pore-Structure Analysis: I—Analysis of Micropores. J. Colloid and Interf. Sci., Vol. 26, 1968, pp. 45-53.
19. Mikhail, R. S., Brunauer, S., and Bodor, E. E. Investigations of a Complete Pore-Structure Analysis: II—Analysis of Four Silica Gels. J. Colloid and Interf. Sci., Vol. 26, 1968, pp. 54-61.
20. Skalny, J., Bodor, E. E., and Brunauer, S. Investigations of a Complete Pore-Structure Analysis: III—Analysis of Carbon Adsorbents. J. Colloid and Interf. Sci., Vol. 37, No. 2, 1971, pp. 476-483.
21. Hagymassy, J., Jr., Brunauer, S., and Mikhail, R. S. Pore Structure Analysis by Water Vapor Adsorption. J. Colloid and Interf. Sci., Vol. 29, No. 3, 1969, pp. 485-491.
22. Pierce, C. Effect of Interparticle Condensation on Heats of Adsorption and Isotherms of Powder Samples. J. Phys. Chem., Vol. 63, 1959, pp. 1076-1079.
23. Emmett, P. H., Brunauer, S., and Love, K. S. The Measurement of Surface Area of Soils and Soil Colloids by Use of Low Temperature van der Waal's Adsorption Isotherms. Soil Sci., Vol. 45, 1938, pp. 57-65.

24. Brunauer, S. The Adsorption of Gasses and Vapors. In Physical Adsorption, Princeton Univ. Press, 1943.
25. Demirel, T. Adsorption of Water Vapor by Sodium and Calcium Montmorillonites. Iowa State Univ., Ames, PhD theses, 1962.
26. Senich, D., Demirel, T., and Handy, R. L. X-Ray Diffraction and Adsorption Isotherm Studies of the Calcium Montmorillonite-H_2O System. Highway Research Record 209, 1967, pp. 23-54.
27. Huang, R. J., Demirel, T., and McGee, T. D. The Adsorption of Water Vapor on E-Glass. J. Am. Ceram. Soc., Vol. 55, No. 8, 1972, pp. 399-405.

PORE STRUCTURE OF FRIABLE LOESS

W. W. Badger, U.S. Army Corps of Engineers; and
R. A. Lohnes, Iowa State University

•THE SIZE, shape, and arrangement of mineral grains composing a soil mass, referred to as structure, have profound influence on the engineering behavior of soil. Many soil mechanicians have recognized the relation of structure to soil shear strength as exemplified by Henkel (6) who, in discussing clay strength, stated: "Some model for the clay structure has to be found which will enable the deformations and pore pressures to be related in a consistent and satisfactory manner."

Other engineering aspects of soil structure involve sensitive soils, compressibility, and permeability. The loss of strength between the undisturbed and the remolded states in sensitive soils is explained as a difference in structure because the density is the same in both cases. The void ratio log pressure curves resulting from confined compression tests on sensitive soils are very flat in the low-pressure range but drop precipitously in the high-pressure range, which has been interpreted as the collapse of soil structure when a critical pressure is reached. At low densities, loess has considerable variation in permeability for a constant density or void ratio as shown by Badger (2). Although a portion of that scatter is due to experimental error, additional scatter is explained as the result of structural differences.

Two serious limitations arise in a study of soil mechanics and structure: One is that the structure is ill-defined, and the other is that soil structure lacks adequate quantification. This paper addresses those 2 general problems and provides some descriptive data for friable loess. A fabric factor has been developed that provides a concept that may contribute to a quantitative classification of soil structure.

DEFINITIONS OF SOIL STRUCTURE

Jenny (9) pointed out that there is no generally accepted definition of soil and that a definition that would satisfy all soil workers is practically impossible to find. The problems inherent in defining soil structure are basically the same as those encountered in defining soils. With the varying interest of geologists, pedologists, and engineers studying soil structure, it is no wonder that there are so many different definitions.

Three terms occur in descriptions of size, shape, and arrangement of soil particles. Structure, fabric, and texture are sometimes used as synonyms but more often have differences in meaning. Various points of view regarding that terminology can be found in the Soil Survey Manual of the U.S. Department of Agriculture (19), the glossary of geological terms published by the American Geological Institute (1), and textbooks on soil physics (3, 4) and on soil mechanics (18).

There is also little agreement on what a particle is or on how particles go together. Therefore, the following definitions, which are close to those of Brewer (4), will be used in this paper:

1. Sand grains, silt grains, and clay crystals are considered as primary soil particles;
2. A composite particle is composed of primary particles that are joined together by some cohesive force;
3. Soil structure is the size, shape, and arrangement of primary or composite particles or both;

Sponsored by Committee on Physicochemical Phenomena in Soils.

4. Fabric is one aspect of structure that describes a specific arrangement involving elements such as lineations; and
5. Texture is a qualitative term for describing particle size (e.g., sand or clay) and is another aspect of structure.

Techniques for measuring and quantitatively describing texture are well known. Similarly techniques for measuring particle shape such as sphericity and roundness are common to petrologists although not often used by soil engineers. Void ratio and porosity, in a sense, are measures of structure or fabric in that they quantitatively describe the void volume in the soil mass. However, if a given void volume is distributed as a few large pores rather than many small ones, the engineering behavior of the soil will differ. Those considerations suggest that measures of pore-size distribution should be helpful in quantifying soil fabric.

PORE-SIZE DISTRIBUTION

Some engineers (12, 16) have used thin sections and light microscopy for soil-structure studies in conjunction with soil mechanics. Lafeber (11) suggested using petrographic techniques such as equal-area spherical projections as a means of quantifying soil fabric. Unfortunately, many undisturbed soils do not possess the lineations of particles or voids that make this technique so successful in petrography.

A significant advance in soil-structure studies was made by Diamond and his associates who demonstrated that mercury-injection porosimetry can be used to characterize the pore-size distribution of soils and to provide a better understanding of engineering modifications of soil such as compaction (5, 17).

That technique is based on the Washburn (20) equation, which gives the pressure required to force mercury into capillary pores.

$$P = \frac{-2\ T \cos \theta}{r}$$

where P is pressure, T is surface tension, θ is angle of contact, and r is radius of pore. After oven-drying and weighing, the sample is placed in the mercury-injection chamber where a vacuum pump removes the pore gases. Although oven-drying of most soils results in shrinkage, which may alter the pore-size distribution, the shrinkage of friable loess due to oven-drying is less than 1 percent by volume. Then the chamber is filled with mercury, and at increments of pressures the volume of mercury intruded into the pores is measured. From the pressures obtained, pore size and volumes may be determined (15). Purcell (13) used an apparatus to determine mercury capillary pressures as high as 2,000 lb/in.^{2}, which filled all accessible pores with radii larger than 5.3×10^{-6} cm (533 Å); that apparatus is similar to the equipment used in this study. Winslow and Shapiro's (21) hydraulic mercury-intrusion porosimeter was capable of pressures of 3,000 lb/in.^{2}. Diamond (5) used a modified Aminco-Winslow porosimeter that has a measuring capacity of 15,000 lb/in.^{2} and can measure pore radii down to 7.11×10^{-7} cm (71 Å).

Both Diamond (5) and Sridharan et al. (17) point out the limitations of the mercury-injection technique and the relation of mercury injection to capillary condensation, which measures void size distributions from 16 to 200 Å. The size distribution of those very small pores has important ramifications in terms of the surface chemistry and physicochemical behavior of clays; however, when gross engineering behavior of soils is studied, such as compaction, deformation, or permeability, those pores are probably not so important, for they reflect the intraparticulate behavior rather more than interparticulate behavior.

In this study of friable loess, 86 percent by weight of the particles are silt size or larger, so the comparatively low-pressure mercury-injection apparatus used here was considered adequate. Huang and Demirel (8) in a companion study used the capillary condensation technique to provide some fundamental data on the very small pore distribution in an undisturbed sample of friable loess.

The soil used in this research was loess obtained from Prospect Hill in Sioux City, Iowa, near the intersection of Bluff and Prospect streets on a large bluff adjacent to

the Missouri River floodplain. The physical properties of the loess are given in Table 1. It is a silty loess according to the classification by Holtz and Gibbs (7) or a friable loess when considered in terms of relative plasticity.

Undisturbed samples were obtained by forcing thin-walled steel Shelby tubes into the soil by the use of hydraulic jacks and by hand-carving soil from the face of the bluff. Samples were collected at depths of about 4 ft below the surface.

The remolded samples were statically compacted in a cylindrical mold ½ in. in diameter and 1 in. in length. The soil was weighed to give a predetermined density and then statically compressed to the standard volume. Samples were similarly molded to Harvard miniature size for permeability and unconfined compression tests.

The mercury-injection apparatus is composed of essentially 3 components: the mercury displacement pump, the sample chamber, and the pressure manifold system (Fig. 1). Purcell (13) gives a more detailed treatment of the type of porosimeter used in this study.

The oven-dried specimen was placed in the porosimeter chamber where a vacuum of 30 μm was obtained. Twenty minutes is usually required to remove most of the entrapped air and moisture from the loess sample.

Mercury was introduced into the chamber so that it completely surrounded the specimen. When the mercury level reached the upper reference mark and the chamber was under 30-μm pressure, the 0-psia reading was taken. At that point the vacuum pump was stopped, and 5 psia of nitrogen was applied to the mercury in the chamber. At predetermined pressure increments, the nitrogen forced the mercury into the loess sample; and the volume of mercury forced into the specimen was recorded at each increment of pressure up to 2,000 psia.

When the loess sample was removed, each specimen was visually inspected. In no case was any sample crushed or damaged; however, the sample shrunk 0.8 percent by volume, and each sample appeared to be completely saturated with mercury when broken apart.

The loess specimens were weighed before and after drying to determine the molding moisture. The remolded cylindrical specimens were measured, and the total volume was calculated. The dry weight and total volume were used to determine a dry density for each specimen.

The total volume of the specimens could be determined by subtracting the volume of mercury introduced into the chamber with the sample in it from the total volume of the chamber at a pressure of 0 psia. However, because of possible errors due to a minute amount of dissolved air in the mercury, that method of total volume measurement was discarded in favor of measuring the gross geometry of the samples. From that volume and the dry weight of the samples, the void ratio was computed. Prior to their placement in the porosimeter, the pieces that were broken from the larger samples were weighed, and the volume of solids was computed by the use of the specific gravity of 2.7. The void volume of the small piece was computed from void ratio and volume of solids.

The mercury volumes measured at the different pressures were corrected for mercury compressibility. The 2,000-psia pressure was used as the upper limit in most tests; however, a few tests were conducted at 1,600 and 1,800 psia. The pressures were converted to radius of pores by use of the Washburn equation, and the data were plotted as pore volume intruded per unit weight versus pore diameter. Cumulative curves were generated by dividing the volume of mercury injected into the sample per pressure-radius increments by the total void volume and then multiplying by 100 to obtain percentage of void volume per total void volume.

The selection of a contact angle and surface tension value was made after an extensive literature search (14, 13, 21, 10, 5, 17). The values of 140 deg and 480 dynes/cm appear reasonable values for minerals in loess. Oven-drying at 105 C for days prior to pumping and waiting 20 min for the pumping down of the 30-μm vacuum removed most of the moisture and air from the sample. A correction for the kinetic hysteresis effect was made by allowing the mercury level to stabilize before a reading was taken.

Figure 2 shows the total porosity of loess as calculated from the known weights of soil, volume of the cylindrical mold, and specific gravity of 2.7 and as measured by mercury injection. The 45-deg line represents the line that would indicate complete agreement between the 2 measurements of porosity. The curve demonstrates that at porosities between 0.3 and 0.45 approximately 10 percent of the pore volume is not intruded by the mercury. At porosities of about 0.55, there is a deviation of nearly 30 percent between the 2 porosity calculations.

Mercury-injection tests on undisturbed samples of loess at porosity of 0.494 revealed that from 17 to 22 percent of the available void volume was not intruded by mercury. Huang and Demirel (8) measured the pore-size distribution in an undisturbed loess sample using the sorption isotherm method and found that the pores with diameters less than about 0.1 μm (i.e., below the size range of the mercury porosimeter) constitute 20 percent of the total pore volume. The interpretation is that at the lower porosities about 10 percent of the pores are too small to be intruded by the mercury. At higher porosities, the greater deviation is accounted for in part by the movement of mercury into large voids on the surface of the soil cylinder at 0 psia. As the mercury tends to partially fill those large surface irregularities, both the measured total volume and the void volume are reduced the same amount so that the total porosity is reduced. That deviation may also be due to a limitation in the Washburn equation at that void size.

The comparison of the pore distribution of undisturbed loess and of remolded loess at the same densities is shown in Figure 3. Each curve represents the average of 3 tests and reveals a rearrangement of pore-volume distribution caused by remolding. Remolding eliminated a portion of the larger pores and increased the maximum pore volume peak of the loess from 13 to 20 percent in volume and the pore radius from 2.7×10^{-4} to 5.3×10^{-4}. In general, the undisturbed loess has a more uniform distribution of pore volume. Some engineering implications of the redistribution of voids caused by remolding are a higher permeability and a greater compressibility in the undisturbed loess.

Twelve loess samples were statically compacted in the ½-in. diameter molds to void ratios ranging from 0.427 to 1.431. The 5 curves shown in Figure 4 are representative of the results of all the tests. All samples were compacted with 16 percent moisture content, which is near optimum for standard Proctor density. The pattern shown in Figure 4 is similar to the results of Sridharan et al. (17) in which the voids are eliminated in order of largest to smallest as the density of remolded loess is increased. That is reasonable because the larger voids formed by the arching of individual grains would be the weakest structural link of the soil system. That is seen from elementary considerations of the larger moments developed in larger arches. For a high-density range, the remolded loess samples disclose relatively few differences in void distributions to density changes. In the low-density range, a small change in density generates a relatively large void distribution change.

SOIL FABRIC FACTOR

A common method of describing a soil for engineering purposes is the grain-size distribution curve obtained from sieve and hydrometer analyses. These data compared to cumulative void-size distribution data provide a means to quantitatively describe the soil structure. By converting the amount of mercury injected into the voids to equivalent diameters, accumulating the volume filled, and computing that as a percentage of the total void volume, one can compare the void-size distribution curve to the grain-size distribution curve computed on a volumetric basis (Fig. 5). To convert the grain-size curve from a weight basis to a volume basis requires the assumption that the specific gravity of the loess particles is constant in all size ranges. That assumption probably does not hold in the clay-size range, and the lower portion of the grain-size curve should shift. However, the upper portion and center of the curve will probably move very little. Further, the assumption that cylindrical pores and void-ratio calculations are based on constant solid density introduces some deviations in pore-size distribution. All distributions are relative to assumptions.

Table 1. Properties of friable loess.

Property	Amount
Grain size distribution, percent by weight	
Clay (< 0.002 mm)	14
Silt (0.002 to 0.074 mm)	86
Specific gravity	2.7
Undisturbed dry density, lb/ft^3	85.3
Liquid limit, percent	30
Plastic limit, percent	26
Standard Proctor compaction	
Optimum moisture content, percent	16.5
Maximum dry density, lb/ft^3	109.4
Field moisture content, percent	7 to 10
Drained triaxial strength (at 85.3 lb/ft^3)	
Cohesion, lb/in.^{2}	1.0
Internal friction angle, deg	32.2
Mineralogy	Quartz, calcite, dolomite, feldspar, montmorillonite, and illite

Figure 1. Shell mercury porosimeter.

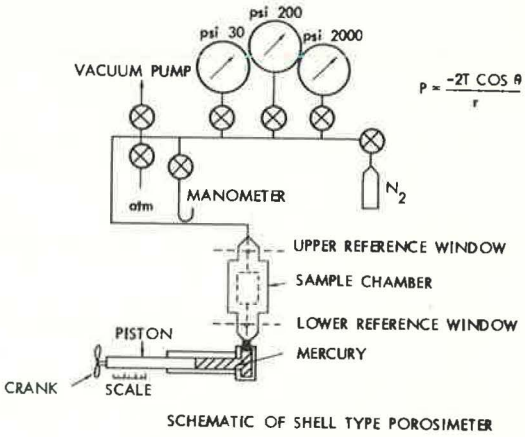

Figure 2. Relation between porosity calculated from bulk density and porosity calculated by mercury injection.

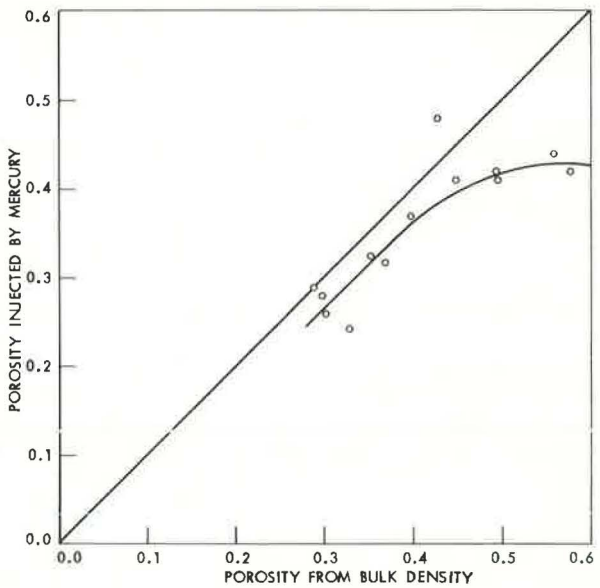

Figure 3. Pore-size distribution of undisturbed loess and loess remolded to field density.

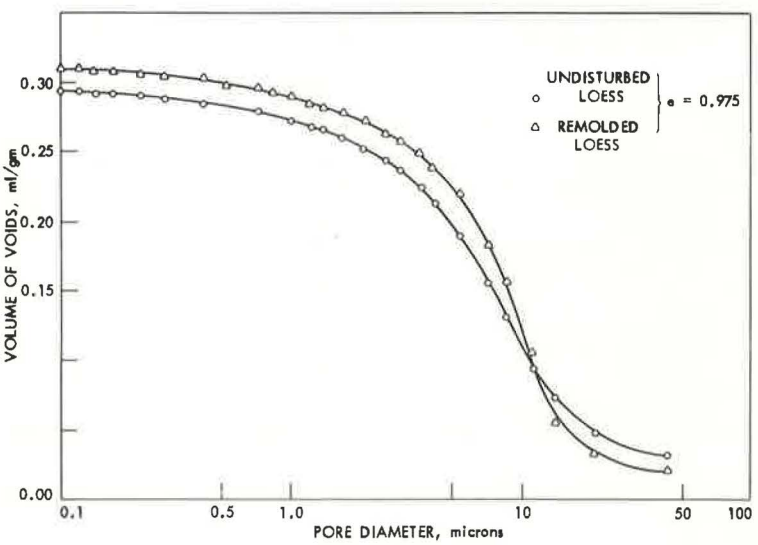

Figure 4. Pore-size distribution of loess compacted to various densities.

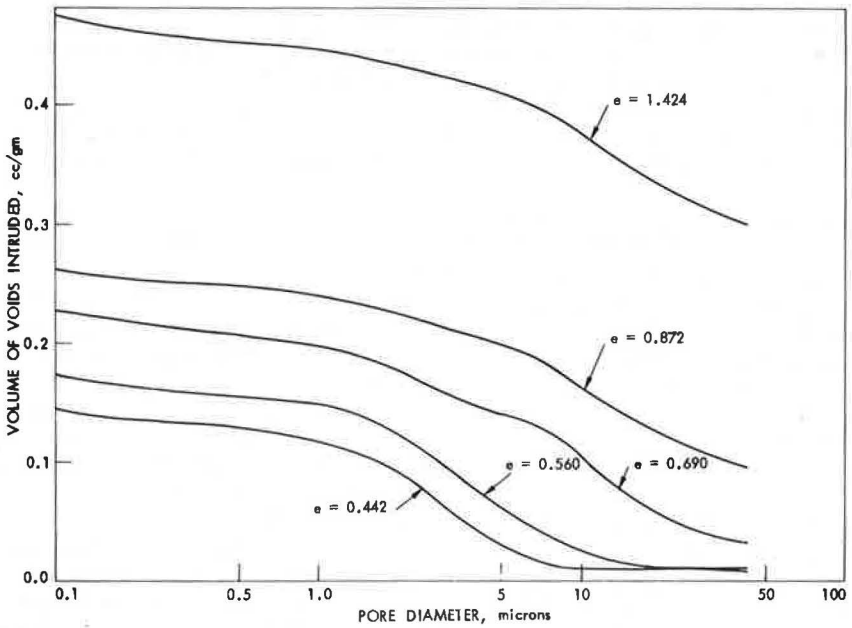

Figure 5. Cumulative pore-size and grain-size distribution as boundaries between various structural classes.

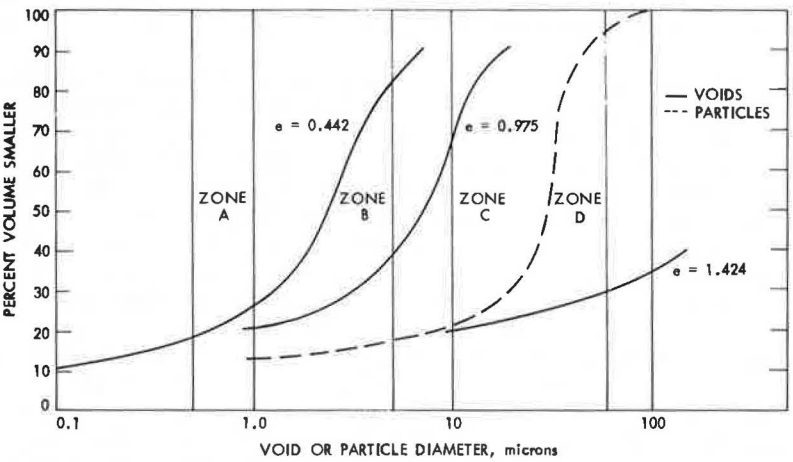

Figure 5 shows the void-size distribution curves for remolded and undisturbed loess plotted with the grain-size distribution curve for loess. At the far left is the void-distribution curve for loess compacted to maximum density at optimum moisture content. The similarity of shapes of the 3 curves is clear and suggests that particle size and shape have a significant influence on the size of the voids.

A conceptual approach to describe soil structure is to use the distribution curves shown in Figure 5 as boundaries for zones. The boundaries are based on observation of loess structure with the scanning electron microscope; micrographs are shown in Figure 6.

The first boundary is the void-size distribution curve for maximum density, the second boundary is the void-size distribution curve for undisturbed loess, and the third boundary is the grain-size distribution curve for loess.

Zone A represents an area above the maximum laboratory density for loess. To attempt higher densities will probably cause crushing of primary particles. Any pore-size distribution curve falling in this zone will be classed as an altered particle structure. No attempts were made to compact loess to that degree.

Zone B represents an area of relatively dense loess (normally higher than the undisturbed or field density) in which primary particles are in contact with each other. Any pore-size distribution curve falling in zone B is designated a particulate structure. The structure shown in Figure 6a is representative of that type of structure.

Zone C represents an area in which many of the primary particles are joined together to form composite particles and 2 classes of voids: the composite void formed among composite particles and the particulate void formed among primary particles. The large composite voids characterize the structure in this zone as shown in Figure 6b. Any pore-size distribution curve falling in that zone is called a composite structure.

Zone D represents the loosest structure where the dominant voids are larger than their adjacent grains and are formed by bridging and arching of composite particles. Figure 6c shows that type of structure. Any void-size distribution curve falling in that area is called a honeycomb structure. Both the altered particle and honeycomb structure classes are more theoretical or limiting structures and will probably rarely occur in loess.

Although the structural zones can be differentiated, a parameter is needed to quantify the structure. A grain-size to void-size ratio at 50 percent fines is defined as the fabric factor. For example, at 50 percent fines on the void-size distribution curve for undisturbed loess, the void diameter is 0.00058 cm. On the grain-size distribution curve, the grain size at 50 percent fines is 0.0031 cm. By dividing the grain diameter of 0.0031 cm by the void diameter of 0.00062 cm, one obtains the fabric factor of 5.43.

Table 2 gives some representative fabric factors for loess and for the soils studied by Diamond and his associates. All of the compacted soils have fabric factors that are greater than one except for the very low-density loess and artificially sedimented kaolinite. It is reasonable, especially in the latter case, that those 2 soils would exhibit a looser structure than soils that have been compacted. A comparison of compacted loess and compacted kaolinite at a void ratio of 0.59 indicates that the fabric factor of the kaolinite is 1½ times larger than that loess. Illite at void ratio of 0.57, on the other hand, has a fabric factor approximately one-third as large as the loess. Undisturbed loess at a void ratio of 0.975 has a fabric factor 20 percent greater than that of compacted loess at the same void ratio. Those comparisons indicate that the fabric factor is sensitive to structural differences in soils and that void ratio alone is unable to measure the difference. Fabric factor systematically decreases as void ratio increases except for the 2 anomolous values at void ratio of 0.975. It should be remembered that the remolded sample was compacted at 10 percent moisture content, whereas the other samples were compacted near optimum moisture content, suggesting that molding moisture also influences structure. For both compacted kaolinite and compacted loess, there is an increase in fabric factor with decreasing void ratio as shown in Figure 7.

Figure 6. Micrographs of 3 structural classes observed in loess.

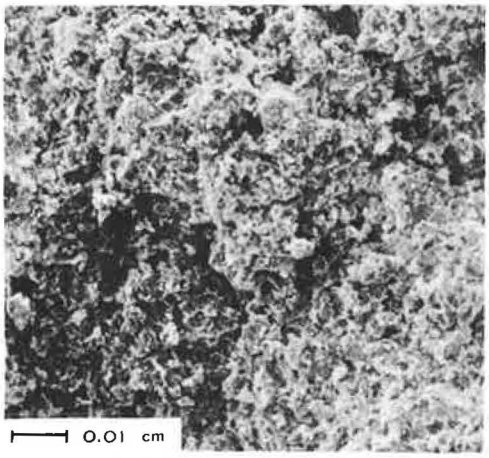

(a) Void ratio = 0.452

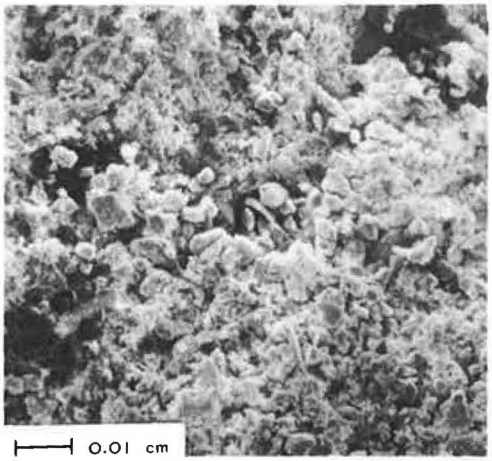

(b) Void ratio = 0.975

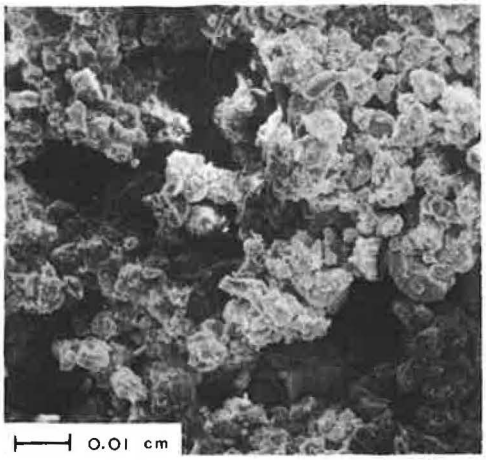

(c) Void ratio = 1.217

Figure 7. Relation between void ratio and fabric factor for loess and kaolinite.

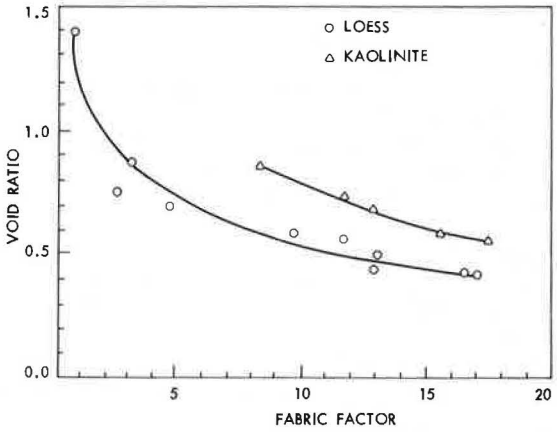

SUMMARY AND CONCLUSIONS

The mercury-injection technique can be used to describe the pore-size distribution of friable loess in both undisturbed and compacted states. The pore-size distribution of samples compacted to essentially the same void ratio as the field condition shows fewer large-sized pores and, in general, a more uniform distribution of pore sizes than the undisturbed samples. Loess samples compacted to various densities at optimum moisture content show trends similar to those observed by Sridharan et al. (17) in that there is a decrease in mean pore size with increasing compaction and that the major reduction in pore volume is achieved by reducing the larger pores.

A comparison of scanning electron micrographs and curves of pore-size distribution plotted on a percentage smaller basis and curves of grain-size distribution reveals that various types of loess structures can be classified. The 3 prevalent structures in loess are the particulate in which primary grains are in contact and the voids are in general much smaller than the grains, the composite in which the primary grains are aggregated into secondary clusters and the sizes of few voids are larger than the grains, and the honeycomb in which the grains form arches over many large voids.

Void ratio and porosity are 2 common parameters used by soil engineers to give some indication of structure; however, a comparison of the data given in Table 2 shows that different soils may have the same void ratio but very different pore-size distributions. The pore-size distribution may be as important as the other parameters, or possibly more so, in explaining the mechanistic behavior of soil insofar as it is one means of quantifying soil structure. Further research is needed to correlate parameters that quantify soil structure with other engineering characteristics.

ACKNOWLEDGMENTS

The authors gratefully acknowledge the support given to this research by the Engineering Research Institute at Iowa State University through funds provided by the Environmental Sciences Division of the Army Research Office. Thanks are also expressed to Turgut Demirel and Lyle Sendlein for their suggestions and constructive criticisms and to the Earth Science Department for making the porosimeter available for this study.

REFERENCES

1. Glossary of Geology and Related Sciences, 2nd Ed. American Geological Institute, Washington, D.C., 1960, 399 pp.
2. Badger, W. W. Structure of Friable Loess in Iowa. Iowa State Univ., Ames, PhD dissertation, 1972.
3. Baver, L. D. Soil Physics, 2nd Ed. John Wiley and Sons, New York, 1948.
4. Brewer, R. Fabric and Mineral Analysis of Soils. John Wiley and Sons, New York, 1964.
5. Diamond, S. Pore Size Distribution in Clays. Clays and Clay Miner., Vol. 18, 1970, pp. 7-23.
6. Henkle, D. J. The Effect of Overconsolidation on the Behavior of Clays During Shear. Geotechnique, Vol. 6, 1956, pp. 139-150.
7. Holtz, W. G., and Gibbs, H. J. Consolidation and Related Properties of Loessial Soils. ASTM, Vol. 126, 1951, pp. 9-33.
8. Huang, R., and Demirel, T. Micropore Size Analysis of Friable Loess. In preparation, 1971.
9. Jenny, H. Factors of Soil Formation. McGraw-Hill, New York, 1941.
10. Klock, G. O., Boersma, L., and DeBacker, L. W. Pore Size Distributions as Measured by the Mercury Intrusion Method and Their Use in Predicting Permeability. Soil Sci. Soc. Am. Proc., Vol. 33, 1969, pp. 12-15.
11. Lafeber, D. Soil Fabric and Soil Mechanics in Soil Micromorphology. In Soil Micromorphology (Jongerius, A., ed.), Elsevier, New York, 1964, pp. 351-360.
12. Mitchell, J. K. The Fabric of Natural Clays and Its Relation to Engineering Properties. HRB Proc., Vol. 35, 1956, pp. 693-713.

13. Purcell, W. R. Capillary Pressures—Their Measurement Using Mercury and the Calculation of Permeability Therefrom. J. Pet. Technol., Vol. 1, 1949, pp. 39-48.
14. Ritter, H. L., and Drake, L. C. Pore-Size Distribution in Porous Materials: Pressure Porosimeter and Determinations of Complete Macropore-Size Distribution. Ind. Eng. Chem. Anal. Ed., Vol. 17, 1945, pp. 782-786.
15. Rootare, H. M. A Short Literature Review of Mercury Porosimetry as a Method of Measuring Pore-Size Distributions in Porous Materials, and a Discussion of Possible Sources of Errors in This Method. Am. Instrument Co., Rept. 439, 1968.
16. Skempton, A. W. Long Term Stability of Clay Slopes. Geotechnique, Vol. 14, 1964, p. 77.
17. Sridharan, A. M., Altschaeffl, A. G., and Diamond, S. Pore Size Distribution Studies. J. Soil Mech. and Found. Div., Proc. ASCE, Vol. 97, No. SM5, 1971, pp. 771-787.
18. Terzaghi, K., and Peck, R. B. Soil Mechanics in Engineering Practice. John Wiley and Sons, New York, 1962.
19. Soil Survey Manual. U.S. Dept. of Agric., Washington, D.C., 1951.
20. Washburn, E. W. Note on a Method of Determining the Distribution of Pore Sizes in a Porous Material. Nat. Acad. Sci. Proc., Vol. 7, 1921, pp. 115-116.
21. Winslow, N. M., and Shapiro, J. J. An Instrument for the Measurement of Pore-Size Distribution by Mercury Penetration. ASTM, Bull. TP 49, 1959, pp. 39-44.

DISCUSSION

Rodney J. Huang and Arshud Mahmood, University of California, Berkeley

The authors have suggested a soil fabric factor—the ratio of median grain size to void size—as a measure of soil structure. The writers feel that the proposed term implies too wide a connotation, for a meaningful description of fabric must also reflect parameters such as gradations and shapes and arrangements of grains and pores. The ratio d_{50}(grain)/d_{50}(pore), or $\bar{L}/\bar{D}$, could more realistically be called "distribution ratio" (2).

Second, the correlation between the fabric term and the state of soil compaction can be improved when d_{50}(pore)/d_{50}(grain) or $\bar{D}/\bar{L}$ is plotted versus porosity instead of void ratio. The writers have added some data on crushed basalt (23) to the authors' data on loess and Sridharan's data on clays (17). The resulting plot is shown in Figure 8. The numbers of the curves are explained as follows:

No.	Reference	Material
1	17	Grundite
2	17	Kaolinite
3	authors	Loess
4	23	Crushed basalt, fines, minus No. 200 sieve
5	23	Crushed basalt, whole, minus No. 8 sieve

It is tempting to speculate that the slopes and intercepts of various straight-line relations reflect mineral grain properties. The points along each line represent different states of compaction. The authors have identified 4 distinct zones in what is essentially a continuous relation between degree of compaction and particle structure. The writers would like to offer schematics based on the authors' SEM photomicrographs representing those 4 zones (Table 3).

Table 2. Fabric factors of loess and other soils at various void ratios.

Soil	Void Ratio	d_{v50}	d_{s50}	Fabric Factor
Loess (compacted)	1.42	>42	31.5	<0.75
Loess (undisturbed)	0.975	5.8	31.5	5.43
Loess (compacted)	0.975	7.6	31.5	4.15
	0.744	12.7	31.5	2.48
	0.591	3.3	31.5	9.55
	0.427	1.8	31.5	17.5
Kaolinite (sedimented)[a]	1.27	2.0	1.4	0.7
Kaolinite (remolded)[a]	0.85	0.17	1.4	8.3
	0.74	0.12	1.4	11.7
	0.69	0.11	1.4	11.7
	0.59	0.09	1.4	15.6
Boston blue clay (compacted)[a]	0.70	0.19	7.0	3.7
Grundite (compacted illite)[a]	0.57	0.37	1.3	3.5

[a]Data from Sridharan et al. (17).

Figure 8. Medium pore-size to grain-size ratio versus porosity.

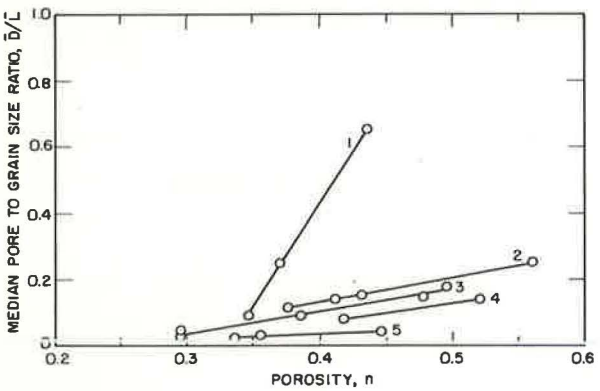

Table 3. Soil structure in relation to compaction effort.

Zone	Structure	Schematic Arrangement	Distribution Ratio	Compaction
A	Altered particle		> 24	Very dense
B	Particulate		24 ~ 6.5	Dense to moderate
C	Composite		65 ~ 1.6	Loose
D	Honeycomb		< 1.6	Very loose

The porosity of a soil can be experimentally related to its strength. One such relationship is given by the exponential equation (22)

$$S = S_o e^{-bn}$$

where

S = strength at porosity n,
S_o = strength at zero porosity,
b = material constant, and
n = porosity.

The logarithmic increase in strength with decreasing porosity is probably a reflection of the exponential variation in the strength of the interparticle forces with changes in the particle spacing. It is suggested that the fabric term introduced by the authors could ultimately be related to the strength of soils by using a relation between porosity and strength. The writers are now attempting such an approach.

References

22. Frydman, S., and Ingles, O. G. The Strength of Cement-Stabilized Fine, Natural Minerals. In Mechanisms of Soil Stabilization, Div. of Soil Mech., Commonw. Sci. and Ind. Res. Organ., Melbourne, 1964, p. 12-1.
23. Mahmood, A. Fabric-Mechanical Property Relationships in Fine Sands. Univ. of California, Berkeley, PhD thesis, 1973.

LATERAL SWELLING PRESSURES IN COMPACTED OKLAHOMA COHESIVE SOILS

Donald Ray Snethen, U. S. Army Corps of Engineers; and
T. Allan Haliburton, Oklahoma State University

ABRIDGMENT

• STRUCTURAL damage resulting from swelling pressures developed in compacted clay soils has been studied and documented by numerous authors. During the early 1960's, several reports (1, 2, 3) indicated that the lateral component (perpendicular to direction of compaction) of those swelling pressures was a primary cause of much of the damage to structures such as foundation walls and buried conduits. Lateral subgrade expansion has also produced tensile stresses in Oklahoma pavement systems of sufficient magnitude to result in longitudinal cracking of pavement components (4).

The purposes of the study described here were to develop instrumentation for direct measurement of lateral swelling pressure of compacted soils and to measure the relative magnitudes of lateral swelling pressure for 2 Oklahoma cohesive soils of moderate to high plasticity and swell potential, as influenced by initial moisture content, dry density, compaction mode and energy, and lateral swell. In addition, vertical swelling pressure data were collected and correlated with lateral swelling pressure data. The sample preparation procedures included varying the compaction mode and energy for initial moisture contents 4 to 6 percent above and below optimum moisture content for the 2 soils. More detailed information is available elsewhere (5).

The lateral swelling pressure was measured by a modified version of a device described by Frost (6). The apparatus, shown in Figure 1, is made entirely of Lucite and has a pressure transducer and strip-chart recorder to measure and record lateral swelling pressure.

A compacted sample surrounded by filter paper and a rubber membrane was placed in the cell, and the cell was filled with de-aired distilled water. Water from the reservoir was introduced to the sample under back pressure, causing the swelling pressure to develop. Because the system was sealed, the water surrounding the sample maintained (for all practical purposes) 0 deformation and transmitted the developed swelling pressure to the pressure transducer, which translated the force to an electric signal for the strip-chart recorder.

Each sample was allowed to take in water and develop swelling pressure until it stabilized at a maximum value. Water was then removed from the Lucite chamber through a burette in the top of the pressure transducer assembly, with resulting lateral expansion of the sample, to allow its swelling pressure to decrease to 0. The system was then resealed, and the swelling pressure was allowed to redevelop. That process was repeated until the incremental lateral swell was so small that essentially no water could be removed.

The influences of initial moisture content, dry density, and compacted soil structure on lateral swelling pressure were found to be highly interrelated for samples compacted with a given compactive effort, as shown by Figure 2. At initial moisture contents below optimum, the trend toward decreasing lateral swelling pressure with increasing initial moisture content is offset by the tendency toward increased lateral

Sponsored by Committee on Environmental Factors Except Frost.

Figure 1. Lateral swelling pressure apparatus.

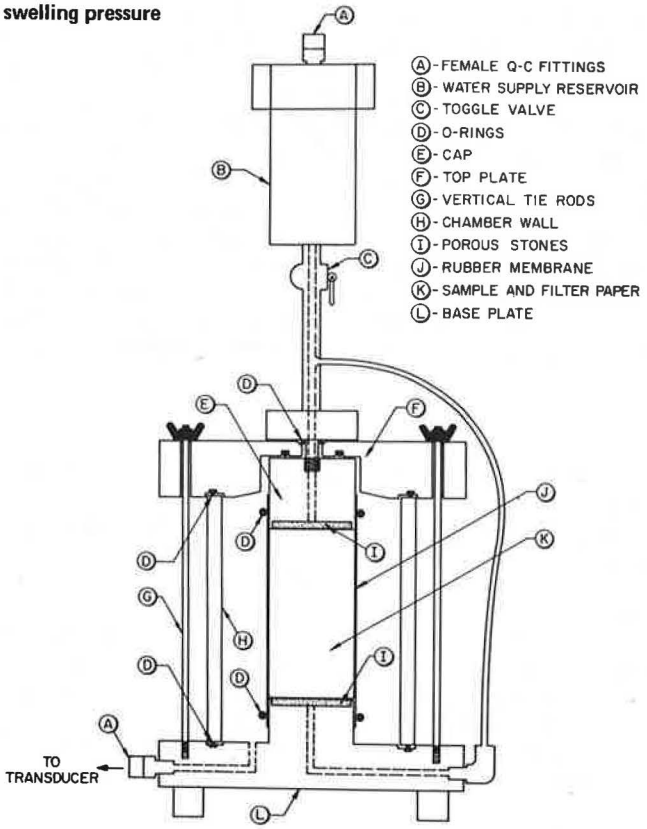

Figure 2. Effect of dry density on lateral swelling pressure.

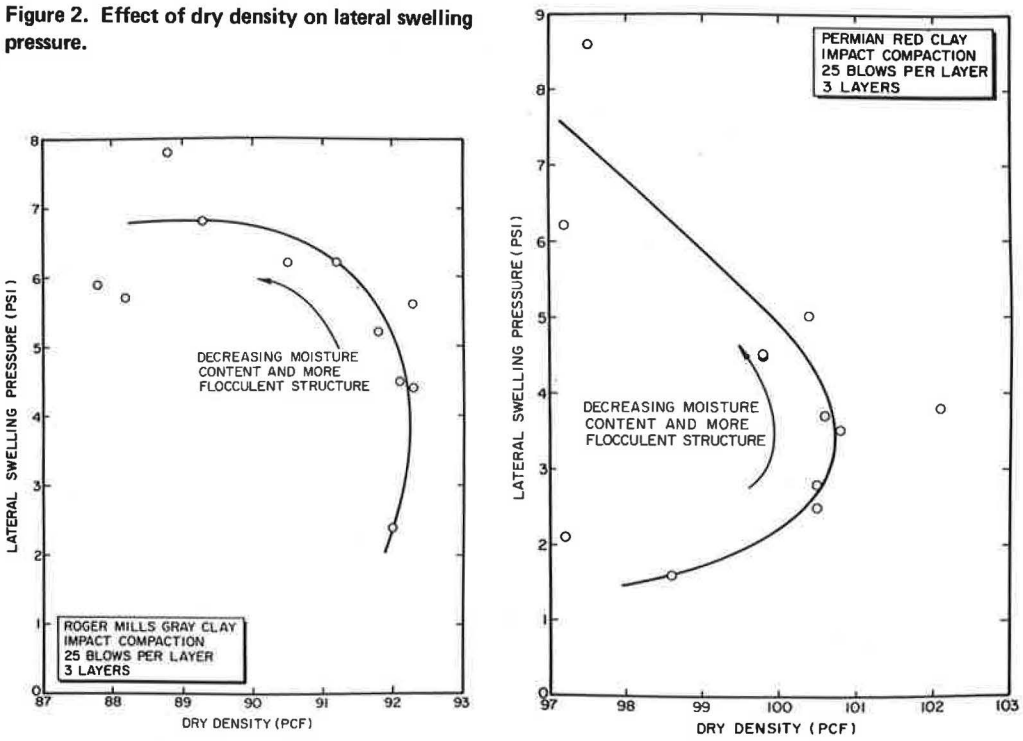

pressure with increasing dry density; thus, a relatively constant magnitude of lateral swelling pressure results. At initial moisture contents slightly below and above optimum, the dry density does not change rapidly, so the effects of moisture content and compacted soil structure determine the swelling behavior. At initial moisture contents above optimum, the influence of increasing moisture content and decreasing dry density combines to reduce the lateral swelling pressure. For both soils, the final moisture content was primarily a function of initial moisture content and was relatively insensitive to dry density. For both soils, the vertical swelling pressure exceeded the lateral swelling pressure for nearly all initial conditions. A maximum lateral swelling pressure of approximately 6.5 lb/in.^{2} was obtained for both soils. The swelling ratio (lateral swelling pressure/vertical swelling pressure) was found to be approximately equal to 1.0 for both soils at moisture contents on the dry side of optimum. At moisture contents above optimum, the swelling ratio is essentially constant between 0.50 and 0.65.

REFERENCES

1. Kassiff, G., and Zeitlen, J. G. Lateral Swelling Pressure on Conduits From Expansive Clay Backfill. HRB Bull. 313, 1961, pp. 1-11.
2. Means, R. E. Buildings on Expansive Clay. Colorado School of Mines Q., Vol. 54, No. 4, 1959, pp. 1-31.
3. Parcher, J. V., and Means, R. E. Soil Mechanics and Foundations. Charles E. Merrill, Columbus, 1968.
4. Haliburton, T. A. Final Report on Subgrade Moisture Variations Research Project. School of Civil Eng., Oklahoma State Univ., Stillwater, Aug. 1970.
5. Snethen, D. R. Lateral Swelling Pressure Relationships for Two Oklahoma Clays. Oklahoma State Univ., Stillwater, PhD thesis, July 1972.
6. Fost, R. B. Development of Equipment for Clay Swelling Tests. Oklahoma State Univ., Stillwater, MS thesis, 1962.

CHANGES IN SOIL SUCTION IN A SAND-CLAY SUBJECTED TO REPEATED TRIAXIAL LOADING

B. Shackel, University of New South Wales, Australia

This paper reports a laboratory investigation that examined whether soil suction values were dependent on the stress history experienced by a soil. Specifically, the effects of repeated triaxial compressive loading on the soil suctions of a kaolinite-sand mixture were studied. The variables examined included the effects of the initial and final dry densities and degrees of saturation and the magnitudes and numbers of the repetitively applied stresses. Both the matrix suctions and the suction-moisture content relations were studied. It was found that the suction values depended primarily on the degrees of saturation but were also slightly influenced by the dry densities. In most cases the effects of repeated loading were to reduce the soil suction corresponding to any given combination of density and saturation; the reduction was greatest at the highest saturations studied. An increase in the number of load applications also tended to reduce the matrix suctions. The work demonstrates the need to consider stress history effects in future investigations of soil suction.

•IT HAS long been recognized that the in-service performance of a pavement is controlled not merely by traffic loadings and initial properties of the pavement materials at placement but also by changes in the subgrade and pavement environments. In many regions of the world, including much of inland Australia and the arid areas of the United States, pavements function in conditions in which the subgrade and base course materials seldom, if ever, become fully saturated. Under those conditions, the effects of the soil environment can, for most practical purposes, be examined in terms of a single fundamental soil property: soil suction.

Many engineering properties of soils including the consistency limits (1, 2, 3), the undrained compressive and vane shear strengths (4, 5, 6), and the CBR's (5, 7, 26) can be related to the corresponding soil suctions. Moreover, limited evidence suggests that the stiffness of soils subjected to both single and repeated stress applications may be related to their suction values (4, 8, 9). Thus, it has been reported that the logarithm of the resilient moduli of repetitively stressed soils increases linearly with increase in the logarithm of their initial suctions (8, 9, 10). In addition, the rate at which residual strains accumulate has been shown to decrease as the initial soil suctions increase (9).

Because of the close interrelation of soil suction with other material characteristics, the observation of suction provides a convenient means of relating the engineering properties of pavement materials to their environment. Consequently, the study of soil suction is assuming an ever-increasing importance in the design of pavements for arid areas (8), the selection of placement conditions for base course materials on expansive subgrades (8, 10, 11), and the prediction of pavement performance (8, 9, 10).

To date most reported investigations of soil suction in pavement materials have ignored the possible influence of stress histories, similar to those experienced in actual pavements, in modifying the suction characteristics. Yet, it has been demonstrated (12) that the action of repetitive stressing on a soil produces complex changes in the soil structure and that the changes manifest themselves as marked alterations in

Sponsored by Committee on Physicochemical Phenomena in Soils.

properties such as stiffness and strength. It is, therefore, reasonable to expect that the suction values measured in a pavement might be modified from their placement values as a result of repeated traffic loadings.

The purpose of the work reported in this paper was to experimentally investigate the influence of repeated triaxial loading on the suction characteristics of a soil exhibiting both internal friction and cohesion. The investigation supplemented previously reported studies of stress-strain and energy dissipation under repeated loading (13, 14, 15, 16).

TEST METHODS

Soil and Specimen Characteristics

Most reported studies of repetitively stressed soils have been restricted to materials in which either the frictional or the cohesive component of shear strength has dominated the soil response. However, in the work reported here, a soil was selected that combined both frictional and cohesive components of shear strength in roughly equal proportions. A uniform sand from Botany, New South Wales, and a commercial air-floated china clay were chosen as the basic materials.

Although there is evidence that, for a given suction, the type of clay minerals present in a soil has little influence on the shear strength (6), the mineralogy of the clay phase nevertheless significantly affects many other engineering properties. The clay phase of the experimental soil was found, by X-ray diffraction and thermal balance analyses, to be a pure kaolinite with slight traces of quartz (less than 5 percent). The kaolinite contained more than 85 percent of particles smaller than 2 μm. Although it was recognized that soils containing kaolinite behave differently from soils containing other clay minerals, the effects of clay mineralogy and physicochemical properties on the soil response could not be studied because the investigation was restricted to just one particular soil.

The work of Paduana (17) on sand-clay mixtures has indicated that, for clay contents between 30 and 50 percent, the relative contributions of the clay and sand fractions to the strength vary approximately with their respective proportions. Based on those findings, a mix showing a slight preponderance of frictional characteristics and composed of 60 percent sand and 40 percent clay, by weight, was selected for the experimental work. The properties of the soil are as follows:

Property	Amount
Liquid limit, percent	26.0
Plastic limit, percent	17.6
Shrinkage limit, percent	14.9
Dry density, lb/ft^3	
Max standard AASHO	112.0
Max modified AASHO	119.5
Optimum saturation, percent	86.5

Specimens of the soil, 4 in. in diameter and 4 in. high, were prepared to designated values of dry density and degree of saturation by the use of floating-mold compaction, a variant of static compaction giving specimens of exceptional uniformity (18). After compaction, each specimen was cured for 3 days at 20 C.

Repeated Load Tests

After being cured, the specimens were subjected to a variety of repeated loads by the use of special equipment described in detail earlier (19). The tests comprised unconsolidated undrained triaxial compression tests with as many as 10,000 repetitions of stress applied in such a manner that the confining stress σ_3 both increased and decreased in phase and in fixed proportion with the axial stress σ_1. This meant that the principal stress ratio σ_1/σ_3 remained constant at all times and that, consequently, the stress paths experienced by the specimens were similar (although not identical) to those

observed in pavements under traffic loadings. The frequency of loading was 2 cpm, and the tests ran for as many as 84 hours, corresponding to 10,000 stress applications. The test temperature was maintained at 20 C.

Measurement of Soil Suction

At the conclusion of each repeated loading test, the soil specimens were broken down by hand into small pieces, each weighing about 10 grams. Representative samples, obtained by a quartering procedure, were used for the determinations of soil suction.

The various techniques for determining soil suctions in the laboratory have been described and critically evaluated elsewhere (1, 20, 21). Only one of those techniques was available to the author: the use of a pressure membrane apparatus of the type developed at the Road Research Laboratory (22). That method is usually considered to be of only moderate accuracy (21) but has the advantage of being relatively simple. That type of equipment is customarily used with null-point method of suction determination (20, 23). That involves the observation of the changes in specimen weight that accompany alterations in the applied air pressures. It then becomes possible to interpolate the pressure and, hence, the soil suction at which water neither enters nor leaves the soil. That procedure largely obviates errors arising from shrinkage and swelling.

In the work reported here it was desired to supplement measurements of the matrix suctions existing at the conclusion of the repeated load tests by observations of the suction-moisture content relations. That precluded the use of a null-point technique. The procedure adopted in the experimental work was, therefore, to first air-dry the soil at 20 C for several days and to subsequently remove the remaining moisture by drying at 45 C under a vacuum of 74 cm of mercury. The relations between suction and moisture content were then defined by measuring the moisture contents corresponding to 8 values of suction, usually ranging between -8 and -60 lb/in.^{2} Values of the matrix suction corresponding to particular values of moisture content could be interpolated from those relations. Thus, all the suction observations lay on the wetting branches of the suction-moisture content hysteresis loops.

For some soils, such as heavy clays, the effect of drying and rewetting the material may be to alter the suction-moisture content relations (5). Thus, the procedures adopted in the work described here carried the risk that they might result in appreciable disturbance of the soil structure. It was, therefore, decided to examine whether drying and rewetting the experimental soil would significantly change the suction values corresponding to various moisture contents. That was accomplished by compacting a number of specimens to a dry density of 115.8 lb/ft^3 at molding saturations ranging between 75 and 95 percent. The moisture contents corresponding to specified suctions ranging between -8 and -60 lb/in.^{2} were then determined for the moist samples. Those suction-moisture content determinations were then repeated after the soil was dried by the procedures detailed above.

The results of this experiment are shown in Figure 1. In general, drying and then rewetting the soil did not significantly alter the moisture contents corresponding to various designated values of suction. It was, therefore, concluded that the experimental procedures did not lead to a significant disturbance in the suctions of the sand-clay soil selected for study.

Control Specimens

Any changes in suction that might result from repeated loading were detected by comparisons of the suction values observed for the repetitively stressed specimens and the values obtained from unstressed duplicate control specimens. The duplicates were compacted, cured, and tested under the same conditions and at the same age as the specimens subjected to repetitive loading.

EXPERIMENTAL WORK

The experimental work comprised 3 interrelated investigations:

1. An examination of the effects of changes in the initial dry density and degree of saturation;
2. An investigation of the effects of load repetition; and
3. A study of the effects of stress history.

Effects of Density and Saturation

The investigation of the effects of initial dry density and degree of saturation on the changes in suction that occurred under the action of repeated loading involved a simple fully randomized, factorial experiment without replication. Two factors, dry density and saturation, were each examined at 3 levels: 112, 115.8, and 119.5 lb/ft^3 (i.e., ranging between standard and maximum modified AASHO densities) for dry density and 75, 80, and 95 percent for saturation. Test specimens were manufactured for all 9 combinations of dry density and degree of saturation. These were supplemented by an additional specimen compacted at a dry density of 115.8 lb/ft^3 and a saturation of 86.5 percent, roughly lying on the "line of optimums." The specimens were then each subjected to 10,000 repetitions of octahedral shear stress τ_{oct} of 5.66 lb/in.^{2} at an octahedral stress ratio τ_{oct}/σ_{oct} of 0.82.

For each of the 10 combinations of density and saturation examined, the suction bore the following relation to the moisture content:

$$h_m = a - b \log_e w \qquad (1)$$

where

h_m = matrix suction, pF;
w = moisture content, percent; and
a and b = empirical constants.

That relation applied equally well to both the repetitively stressed samples and their unstressed duplicates. The empirical constants a and b were evaluated by regression analyses. Values of the correlation coefficient r ranged between 0.78 and 0.98.

Values of the suction parameters a and b, measured after compaction but before the application of any stress history, are shown as functions of the initial (molding) degrees of saturation and the compacted dry densities in Figure 2. By contrast, Figure 3 shows the changes in the suctions and the suction-moisture content relations that resulted from repetitive loading. In general, the effects of repeated loading were to reduce the matrix suctions, and that effect became more pronounced as the molding saturations were increased.

The work of Baver (24) and Russell and Mickle (2) has demonstrated that, in general, soil suction-moisture content relations plot as curves divided into 3 distinct regions by flex points at moisture contents corresponding to the plastic and liquid limits. In the work reported here, the molding moisture contents studied were all dry of the plastic limit. Thus, although the form of Eq. 1 is identical to that reported earlier by Livneh et al. (1), extrapolation of that relation beyond the domain of the experimental observations (or beyond the plastic limit) would not be valid. Consequently, Eq. 1 should be regarded only as a convenient engineering approximation to just part of the true suction-moisture relation, and it would be unwise to attempt to assign any fundamental physical meanings to suction parameters a and b.

In practice, most subgrade and pavement materials are compacted dry of the plastic limit; therefore, it can be argued that simple relations of the form given in Eq. 1 may prove useful in predicting suction-moisture changes. However, such an approach fails to recognize that changes in suction (or moisture content) are usually accompanied by changes in the soil volume (10). Thus, ideally, Eq. 1 should be expanded to include the effects of changes in the voids ratio or dry density.

Adopting that approach, we established that the matrix suction was a function of both the degree of saturation and the dry density and that the suction, density, and saturation relation could be represented as a curved surface. The techniques of multiple linear regression were used to determine that, for the range of densities and saturations ex-

amined, the surface could be closely approximated by a plane. That is shown in Figure 4. The relation for the unstressed soil is shown as plane ABCD. The regression equation describing that plane is

$$h_m = 0.099\ \gamma_d - 0.044\ S_r - 4.49 \quad (2)$$

where

h_m = matrix suction, pF;
γ_d = dry density, lb/ft^3; and
S_r = degree of saturation, percent.

After repeated loading, the suction, density, and saturation relation could be approximated by plane A′B′C′D′ (Fig. 4), which had the equation

$$h_m = 0.135\ \gamma_d - 0.067\ S_r - 7.060 \quad (3)$$

Figures 3 and 4 show that the effects of repeated loading on the matrix suctions became increasingly more pronounced as the molding saturations increased or as the initial dry densities decreased. However, for both the repetitively stressed specimens and the unstressed control specimens, the multiple regression analyses revealed that the degree of saturation S_r was statistically more significant than the dry density γ_d in controlling the matrix suctions. That is consistent with experimental data published earlier (11, 23, 25).

The multiple F values for Eqs. 2 and 3 were 223.7 and 86.97 respectively, with 2 and 7 degrees of freedom. Inspection of tables of critical F shows that, for P(F) = 0.005, there was no significant lack of fit between the regression equations and the experimental data. That does not, of course, imply that the models represented by Eqs. 2 and 3 were fundamentally correct or that they were necessarily the best fits to the experimental data. Nevertheless, the models provided useful predictions of the alterations in suction that resulted from changes in density or saturation as long as those changes did not fall outside the domain of the experimental observations.

Figure 4 shows that the effect of repetitive loading was to substantially alter the suction-density-saturation relation. Thus, a soil, whose initial condition can be represented by point p in plane ABCD, may, as the result of cyclic loading, adopt the state represented by point p″ in plane A′B′C′D′. However, changes in suction need not be accompanied by changes in either density or saturation; i.e., the suction may change along path pq (Fig. 4). That suggests that the observed changes in matrix suction probably arose from alterations in the soil structure caused by repeated loading.

A study of the relations between strength and suction provided further evidence of changes in soil structure. For the control samples, which were not subjected to repeated loading, compressive strengths C were determined to be linearly related to the suctions. That is shown in Figure 5. The regression equation was

$$C = 51.74\ h_m - 97.97 \quad (4)$$

That relation appeared to be independent of both the density and the saturation. However, for specimens that had been subjected to 10,000 load cycles, it was found that the simple relation given in Eq. 4 was no longer valid. Although, as in the case of the unstressed specimens, increases in suction were accompanied by increases in strength, it was not possible to fit a single curve relating strength and suction to the data. Instead it was necessary to plot separate curves for each of the levels of dry density studied (Fig. 5). The suctions and compressive strengths were affected to quite different degrees by repeated loading; therefore, the mechanisms causing strength changes were probably different from those associated with alterations in the matrix suctions. The changes in strength that resulted from repetitive loading have been considered in greater detail elsewhere (12).

As noted earlier, some evidence suggests that the stiffness of repetitively stressed soils may be related to the soil suctions. It was, therefore, decided to investigate whether it would be possible to relate the strains caused by cyclic loading to the cor-

Figure 1. Comparison of suction measurements on moist and dried samples.

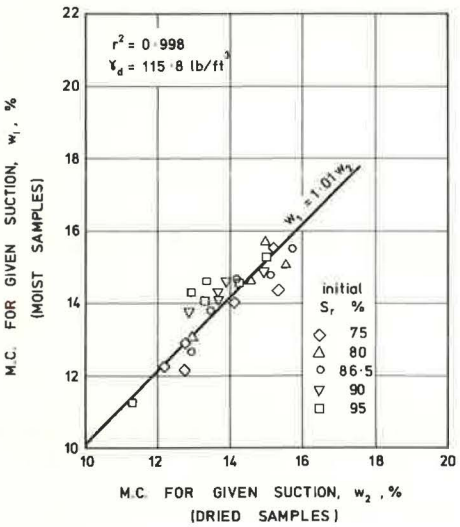

Figure 2. Suction parameters for unstressed control specimens.

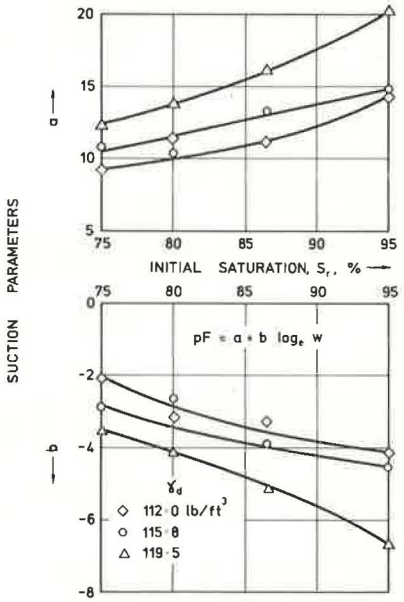

Figure 3. Changes in soil suction resulting from repetitive loading.

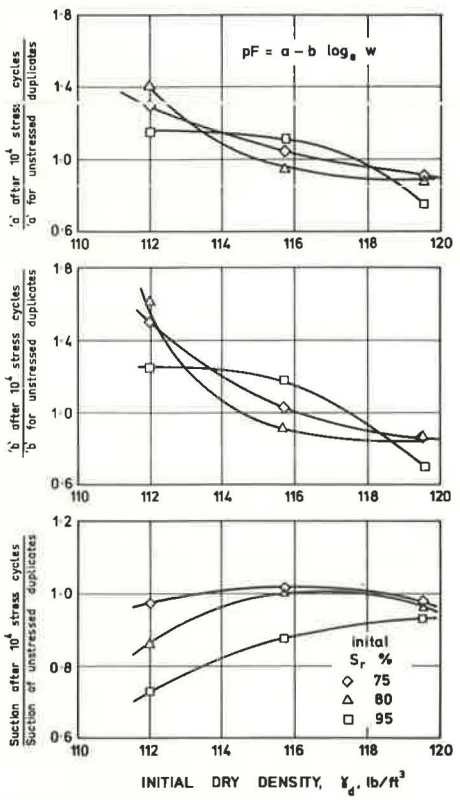

Figure 4. Regression models used to approximate the suction-saturation-density relations.

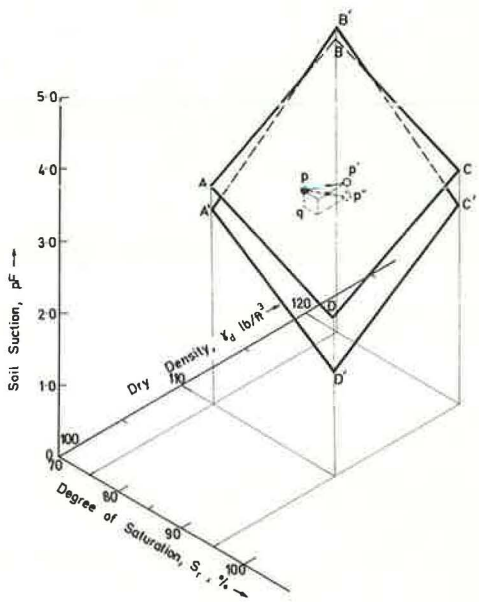

responding matrix suctions. Two axial strain components were examined: resilient strain ϵ_r and cumulative nonrecoverable (plastic) strain ϵ_f.

The relations between resilient axial strains ϵ_r and suctions are shown in Figure 6 for the first and last load cycles. As shown in the figure, it was established that the relations between the resilient strains and the suctions were dependent on the molding saturations and the initial dry densities. The techniques of multiple regression were used to determine the following arbitrary relations among ϵ_r, the suctions, and the degrees of saturation.

For N = 1,

$$\epsilon_r = -75\ h_m - 19.94\ S_r + 4{,}714 \text{ (microstrain)} \quad (5)$$

and F = 3.02 with 2 and 6 degrees of freedom; and for $N = 10^4$,

$$\epsilon_r = -778.3\ h_m - 40.8\ S_r + 6{,}649 \text{ (microstrain)} \quad (6)$$

and F = 9.74 with 2 and 5 degrees of freedom.

Previous stiffness-suction relations (8, 9, 10) have been reported in terms of the suctions measured prior to repeated loading. By contrast the simple models represented by Eqs. 5 and 6 relate the suctions resulting from a given stress history to the corresponding strains. However, the regression models are based on only a limited amount of experimental data. Consequently, although the models are useful in delineating possible stiffness-suction relations, they must nevertheless be treated with caution until their validity can be tested against more comprehensive data than those available to the author.

The relation between cumulative nonrecoverable strains ϵ_f and suctions is shown in Figure 7. Each point represents a different combination of initial dry density and molding saturation. The residual strains resulting from the designated stress history decreased rapidly as the suctions increased. The form of that relation and the form reported earlier by Sauer and Monismith (9) are similar in that the coefficients of residual deformation are related to the initial suctions.

Effects of Load Repetition

The effects of various numbers of load applications were examined in a series of 5 repeated load tests, each terminating at a different number of applications. Five replicate specimens were compacted to a nominal dry density γ_d of 115.8 lb/ft^3 at a degree of saturation S_r of 80 percent. They were then respectively subjected to 1, 10, 100, 1,000, and 10,000 applications of an octahedral shear stress τ_{oct} of 5.66 lb/in.^{2} at an octahedral stress ratio τ_{oct}/σ_{oct} of 0.82.

At the conclusions of the repeated load tests, measurements were made of suction parameters a and b and matrix suctions h_m. Those observations are shown in Figure 8. At low numbers of load applications, the suction parameters measured for the repetitively stressed specimens were significantly higher than the corresponding values measured for the duplicate control specimens. Moreover, the maximum increase in suction occurred during the first load application. Subsequently, however, the suctions tended to decrease with increasing numbers of load applications.

Effects of Stress History

The effects of stress history were examined in an incomplete factorial experiment. The factors investigated were octahedral normal stress σ_{oct} and octahedral stress ratio τ_{oct}/σ_{oct}. Three levels of τ_{oct}/σ_{oct} ranging from 0.82 to 1.07 were studied. Values of octahedral shear stress τ_{oct} ranged between 5.7 and 22.6 lb/in.^{2} The test specimens were each compacted to a dry density of 115.8 lb/ft^3 at a saturation of 80 percent.

The results of that experiment are shown in Figure 9. Varying the stress regime produced complex changes (usually decreases) in the matrix suctions. Those changes were generally smaller than those that accompanied alterations in the density, saturation, or number of load applications. Although for each level of τ_{oct}/σ_{oct} examined the suctions were a minimum at some particular value of σ_{oct}, the author was unable to

Figure 5. Relation between unconfined compressive strength and matrix suction before and after repeated loading.

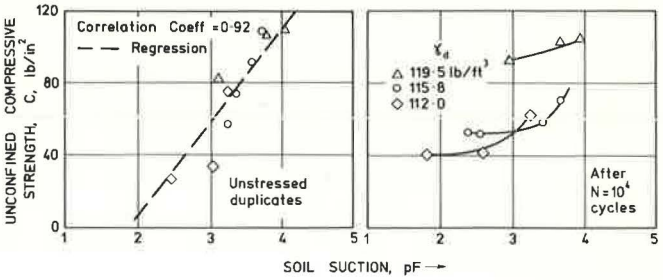

Figure 6. Relation between resilient axial strains and matrix suctions.

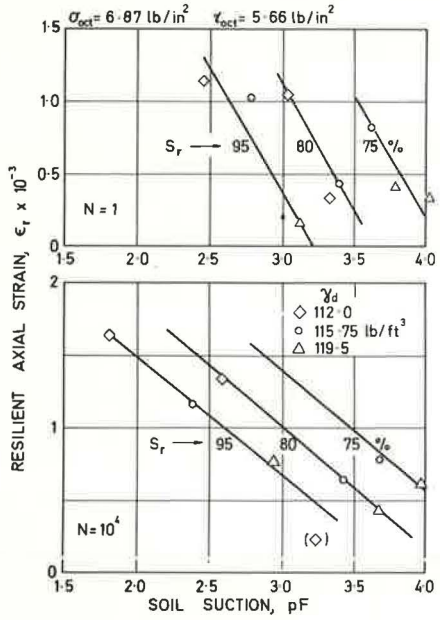

Figure 7. Relation between the nonrecoverable strains and final matrix suctions.

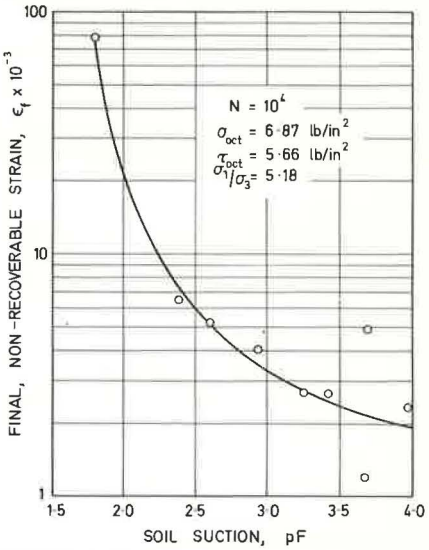

Figure 8. Effects of load repetition on soil suctions.

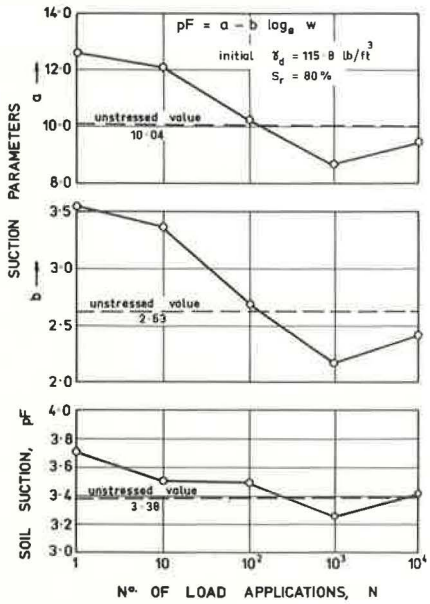

Figure 9. Influence of stress history on final matrix suctions.

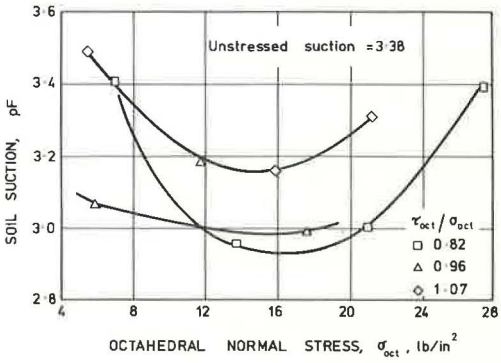

determine whether it was possible to relate the suctions measured after repeated loading to the magnitude of the repetitive stresses. Moreover, there did not appear to be any obvious relation between the suctions and the corresponding strains or compressive strengths.

SUMMARY AND CONCLUSIONS

The work reported here demonstrated that the suctions exhibited by a compacted soil were functions not merely of the moisture content and dry density at compaction but also of the stress history experienced by the soil. A summary of the principal conclusions of the experimental investigation follows.

1. The matrix suctions h_m of both the repetitively stressed samples and the unstressed control specimens were primarily a function of the degree of saturation but also slightly depended on the dry density. In general, the suctions increased with increase in density or with reduction in saturation.
2. The effects of repeated triaxial loading were usually to decrease the suction corresponding to any given combination of dry density and degree of saturation. The decreases in suction could largely be attributed to changes in the soil structure.
3. For both the repetitively stressed samples and the control specimens, the matrix suctions could, for the range of densities and saturations studied, be related to changes in the moisture content by expressions of the form

$$h_m = a - b \log_e w$$

The effects of repeated loading were to alter the coefficients a and b.
4. The magnitude of the changes in soil suction resulting from repetitive loading tended to increase as the initial (molding) saturations were increased.
5. As the numbers of stress applications applied to a sample were increased, the final suctions tended to decrease.
6. Alterations in the stress regime produced slight alterations in the final suction values; however, those changes were smaller than those associated with alterations in density or degree of saturation.
7. For a particular molding saturation, the resilient axial strains decreased linearly with increase in the suctions, expressed in pF units.
8. The cumulative, nonrecoverable (residual) axial strains decreased rapidly as the suctions increased.

Elsewhere, Richards (26) has drawn attention to the fact that soil suction measurements are, in effect, measurements of potential that obey hydrodynamic and thermodynamic laws. It is of interest, therefore, to examine whether there are any relations between the changes in soil suction resulting from some given stress history and the corresponding expenditures in strain energy. The author has already reported some of the changes in the input and damping strain energies that occurred in the experimental soil during the various repeated load tests (13, 27); it has been found possible to qualitatively relate those changes to the alterations in soil suction.

It was determined that, with increasing dissipation of the loaded input strain energy, the suctions tended to decrease. Moreover, it was observed that both resilient and residual strains occurring in any cycle of loading and unloading often tended to decrease as the damping energies decreased. Because soils continue to dissipate part of the input strain energy even when the deformations are completely recoverable, it would be expected that, in general, the suctions would tend to steadily decrease with increase in the numbers of stress repetitions. Except for a few tests in which the suctions increased slightly, that type of behavior was observed throughout the experimental work, and conclusions 5 to 8 can, at least in part, be explained in terms of energy changes. However, to derive valid, quantitative, thermodynamic soil relations that include both suction and strain energy parameters has not yet proved to be possible.

Dry densities and saturations of the soil specimens and stress paths and stress levels used in the repeated load tests were all carefully chosen to be as nearly rep-

resentative of actual pavements as could be conveniently achieved in the laboratory. Therefore, real pavement materials probably would exhibit changes in soil suction similar to those observed in this study. However, it is important to recognize that the changes in soil suction reported here were produced in a test lasting only 3½ days. By contrast, similar changes in a pavement might take several months or even years to complete. The significance of the suction changes observed under laboratory conditions may, therefore, be different from those occurring in situ, and further research is needed on that aspect of the problem.

REFERENCES

1. Livneh, M., Kinsky, J., and Zaslavsky, D. Correlation of Suction Curves With the Plasticity Index of Soils. J. Mater., Vol. 5, No. 1, 1970, pp. 209-220.
2. Russell, E. R., and Mickle, J. L. Liquid Limit Values by Soil Moisture Tension. Proc., ASCE, Vol. 96, No. SM3, 1970, pp. 967-989.
3. Russell, E. R., and Mickle, J. L. Correlation of Suction Curves With the Plasticity Index of Soils. J. Mater., Vol. 6, No. 2, 1971, pp. 320-331.
4. Aitchison, G. D. The Strength of Quasi-Saturated and Unsaturated Soils in Relation to the Pressure Deficiency in the Pore Water. Proc., 4th Int. Conf. Soil Mech. and Found. Eng., Vol. 1, 1957.
5. Croney, D., Coleman, J. D., and Black, W. P. M. Movement and Distribution of Water in Soil in Relation to Highway Design and Performance. HRB Spec. Rept. 40, 1958.
6. Dumbleton, M. J., and West, G. The Suction and Strength of Remoulded Soils as Affected by Composition. Gt. Brit. Road Res. Lab., Rept. LR 306, 1970.
7. Morris, P. O. Moisture Movement Under Roads in a Black Soil Area of Western Queensland. Aust. Road Res., Vol. 2, No. 1, 1964, pp. 27-45.
8. Richards, B. G. The Role of Environment in Flexible Pavement Design. Trans. Inst. Eng. Aust., Vol. CE10, No. 2, 1968, pp. 197-205.
9. Sauer, E. K., and Monismith, C. L. The Influence of Soil Suction on the Behavior of a Glacial Till Subjected to Repeated Loading. Highway Research Record 215 1968, pp. 8-23.
10. Richards, B. G., and Gordon, R. Prediction and Observation of the Performance of a Flexible Pavement on an Expansive Clay Subgrade. Proc., 3rd Int. Conf. Struct. Des. of Asphalt Pavements, London, Vol. 1, 1972, pp. 133-143.
11. Richards, B. G., Murphy, H. W., Chan, C. Y. L., and Gordon, R. Preliminary Observations on Soil Moisture and "Dry" Compaction in Pavement Design on the Darling Downs, Queensland. Proc., 5th Conf. Aust. Road Res. Board, Canberra, Vol. 5, Pt. 5, 1970, pp. 116-146.
12. Shackel, B. Changes in the Behavioural and Structural Characteristics of a Repetitively Stressed Sand-Clay. Proc., 6th Conf. Aust. Road Res. Board, Canberra, Paper 910, 1972.
13. Shackel, B. Measurement of Soil Damping Characteristics Using Cyclic Loading Triaxial Equipment. Proc., 4th Asian Reg. Conf. Soil Mech. and Found. Eng., Bangkok, Vol. 1, 1971, pp. 221-226.
14. Shackel, B. The Deformation Response of a Sand-Clay Subjected to Repeated Triaxial Compressive Stress. Proc., Int. Symp. Strength and Deform. Behav. of Soils, Bangalore, Vol. 1, 1972, pp. 145-149.
15. Shackel, B. Linear and Non-Linear Models of the Stress-Strain Response of a Cyclically Stressed Soil. Proc., 3rd Southeast Asian Conf. Soil Eng., Hong Kong, 1972.
16. Shackel, B. The Derivation of Complex Stress-Strain Relations. Proc., 8th Int. Conf. Soil Mech. and Found. Eng., Moscow, 1973.
17. Paduana, J. A. The Effect of Type and Amount of Clay on the Strength and Deformation Characteristics of Clay-Sand Mixtures. Univ. of California, PhD thesis, 1966.
18. Shackel, B. The Compaction of Uniform Replicate Soil Specimens. Aust. Road Res., Vol. 4, No. 5, 1970, pp. 12-31.

19. Shackel, B. A Research Apparatus for Subjecting Pavement Materials to Repeated Triaxial Loading. Aust. Road Res., Vol. 4, No. 4, 1970, pp. 24-52.
20. Aitchison, G. D., and Richards, B. G. A Broad-Scale Study of Moisture Conditions in Pavement Subgrades Throughout Australia. Proc., Symp. Moisture Equilibria and Moisture Changes in Soils Beneath Covered Areas, Butterworths, 1965, pp. 184-323.
21. Engineering Concepts of Moisture Equilibria and Moisture Changes in Soils. Proc., Symp. Moisture Equilibria and Moisture Changes in Soils Beneath Covered Areas, Butterworths, 1965, pp. 7-21.
22. Coleman, J. D. An Investigation of the Pressure Membrane Method for Measuring the Suction Properties of Soils. Gt. Brit. Road Res. Lab., Rept. 3464, 1959.
23. Morris, P. O., Tynan, A. E., and Cowan, D. G. Strength, Density, Moisture Content, and Soil Suction Relationships for Grey-Brown Soil of Heavy Texture. Proc., 4th Conf. Aust. Road Res. Board, Melbourne, Vol. 4, Pt. 2, 1968, pp. 1064-1082.
24. Baver, L. D. Soil Physics, 3rd Ed. John Wiley and Sons, New York, 1956.
25. Olson, R. E., and Langfelder, L. J. Pore Water Pressures in Unsaturated Soils. Proc., ASCE, Vol. 91, No. SM4, 1965, pp. 127-150.
26. Richards, B. G. Moisture Flow and Equilibria in Unsaturated Soils for Shallow Foundations. ASTM, Philadelphia, STP 417, 1967, pp. 4-34.
27. Shackel, B. The Effects of Stress and Environmental Factors on the Damping Response of a Cyclically Stressed Sand-Clay. Symp. Behav. of Earth and Earth Struct. Subjected to Earthquakes and Other Dynamic Loads, Roorkee, 1973.

FROST-SUSCEPTIBILITY CRITERIA

H. L. Jessberger, Institute of Soil Mechanics and Foundation Engineering,
Technical University, Munich

•A SURVEY of frost-susceptibility criteria shows that those now in use can be divided into 3 groups based on the following characteristics:

1. Gradation curves and particle size,
2. Frost-heave rate, and
3. Phase-interface relation.

Groups 1 and 2 are empirical, and group 3 has a theoretical basis.

The existing frost-susceptibility criteria do not meet the demand of characterizing the soils with regard to frost action in the form of quantitative values. A more scientific approach encompassing complex variables is desired in order to define frost susceptibility. Manual testing procedures developed for rapidly detecting the frost susceptibility in situ are not described in this paper.

PARTICLE-SIZE CRITERIA

The most common method for determining the frost susceptibility is to plot the grain-size gradation curve and to compare the content of fines against some arbitrarily fixed values. Those values have been found by a series of field investigations at locations where frost damages occurred. The criteria formulated by Casagrande or by Schaible are typical examples of that procedure.

Table 1 (1) gives the limiting values of certain particle sizes listed according to different authors.

In the United States and several other countries, the Casagrande criterion is very often incorporated in the design of pavement (2, 3). However, soils conforming to the Casagrande criterion under certain conditions may show detrimental frost effects. On the other hand, any transgression of that criterion does not automatically lead to frost damages. Several of the United States have, therefore, established their own criteria based on experience and field investigations. Haley (4) reported that in Massachusetts soils with more than 15 percent passing the No. 200 sieve are considered frost susceptible, whereas in Delaware the limit is fixed at 35 percent.

Other authors (5, 6) have proposed to classify soils as having a tendency toward frost susceptibility rather than as being or not being frost susceptible.

The authors mentioned above have considered the particle-size distribution to be of paramount importance in influencing the frost susceptibility of a given soil. Other factors, such as soil minerals, chemical conditions, surcharge load, water table, and temperature gradients, have not been considered. For that reason, the particle-size criteria should not be used in geological formations and regions with climatic and hydrological conditions different from the conditions existing at the places where those criteria have been established and their validity confirmed.

The fact that the "bearing capacity" of a soil is lower after thaw than in the fall season suggests that the modulus of elasticity should be reduced accordingly in the design of pavements (7, 8). In other words, the bearing capacity after thaw has been given due consideration in addition to the grain-size distribution of a soil. Further advances in that direction show that the bearing capacity after thaw is controlled by

Sponsored by Committee on Frost Action.

the particle content <0.02 mm and the uniformity coefficient (9). The influence of other factors, such as soil minerals, chemical composition of the soil, climatic conditions, and water availability, on the test results are not yet known.

FROST-HEAVE RATE CRITERIA

Frequently the frost-heave rate serves as a gauge for the influence of various conditions, such as temperature, surcharge load, and water availability (tests in open or closed systems), on the frost susceptibility of a soil. Frost-heave rate is used especially in checking the efficiency of additives in stabilized soils because in stabilized soils the particle-size criterion has no validity.

Frost-heave tests have been made only with small-scale models that simulate the in situ conditions. The model laws, however, are not yet known. The few efforts made to detect them have not led to a definite conclusion, and controversy still exists concerning the influence of temperature gradient to heave rate (10, 11).

Therefore, a direct application of the results of heave-rate tests to road design against frost action is not recommended. That can be done only when the test procedure has been standardized in detail and a frost-susceptibility classification has been established by comparison of frost-heave rates found in laboratory tests with observations made at the site. The Road Research Laboratory (12) and the U.S. Corps of Engineers (3) have worked in that direction. The frost-susceptibility classification developed by the Corps of Engineers is as follows:

Avg Frost-Heave Rate (mm/day)	Frost Susceptibility
< 0.5	Negligible
0.5 to 1.0	Very low
1.0 to 2.0	Low
2.0 to 4.0	Medium
4.0 to 8.0	High
> 8.0	Very high

It is not known that the model law is linear; therefore, that classification can be used only if the conditions at a new construction site coincide with the general conditions at sites where comparisons between laboratory and field investigations have been made. Results of comparisons of untreated soils would, of course, not be applicable to stabilized soils.

The frost-heave rate gives information on the soil behavior during freezing only and neglects the critical stage of thawing when the bearing capacity is at its lowest. The recently developed test method for recognizing the loss in bearing capacity (9) consists of subjecting soil samples to several freeze-thaw cycles. The frost-heave rates found during freeze periods are not identical with data obtained by using the method of the Corps of Engineers (3), but the tendency is the same. Table 2 gives the frost-heave rate of a few soils and CBR after the last thaw period (9). The index properties of the soils as well as their origin are described in another report (9). A direct relation between frost-heave rate and CBR after thaw does not exist. Here again consideration has been given to grain-size distribution. The data given in Table 2 show that the lesser the uniformity of the soil is, the smaller the bearing capacity is because the fine material is responsible for the frost effect and the coarse material is mainly responsible for the residual bearing capacity (compare soil 16 and soil 4, Table 3). Frost-heave rates alone give no information on that behavior.

The importance of incorporating the CBR value in the frost-susceptible criteria is shown in Figure 1. Although the heave rates during freezing and settlements during thawing are similar for the ETS and MSI soils, the CBR values are in the ratio of 14:1. The grain-size distribution curves of the ETS and MSI soils are shown in Figure 2.

Balduzzi (13) states that the bearing capacity is to be taken as a basis for pavement design. He considers the frost-heave rate test to be valuable in recognizing the "stability" of soils against frost effect. In other words, the "instability" of frost-susceptible

Table 1. Particle-size frost criteria according to content of fines.

Author	Fine Content	Percentage by Grain Size (mm)					
		<0.125	<0.1	<0.062	<0.05	<0.02	<0.002
Beskow	Uniform	22-35		15-25			
	Nonuniform			33-50			
Kögler-Scheidig[a]	Uniform					3	
	Nonuniform					10	
Morton[b]					10		
Casagrande[c]	Uniform					3	
	Nonuniform					10	
Schaible	Frost susceptible		20			10	1
	Highly frost susceptible		40			20	6

[a]If free water is available, the frost susceptivity is classed by means of the permeability: k = 1.10^{-6} to 1.10^{-7} m/sec, highly frost susceptible; k = 1.10^{-7} to 1.10^{-8} m/sec, frost susceptible; and k (1.10^{-8} m/sec, not frost susceptible.
[b]Valid only for soils with particle diameter between 0.001 and 2.0 mm.
[c]According to Dücker not applicable, for vulcanic soils and for very uniform soils.

Table 2. Frost-heave rate and CBR after thaw for 4 soils.

Soil	Frost-Heave Rate (mm/day)	CBR After Thaw (percent)	Particle Content <0.02 mm (percent)	Uniformity Coefficient d_{60}/d_{10}
16 ETS	42.4 (13.7)	11.7 (8.7)	9.0	54.5
1 MSI	32.1 (13.4)	0.63 (0.62)	65	3.0
1 HPG	21.0	31.7	5.5	29.3
4 HSS	19.1	7.3	7.1	6.3

Note: Numbers in parentheses are test results according to Figure 1.

Figure 1. Temperature and vertical movement during freeze-thaw cycles.

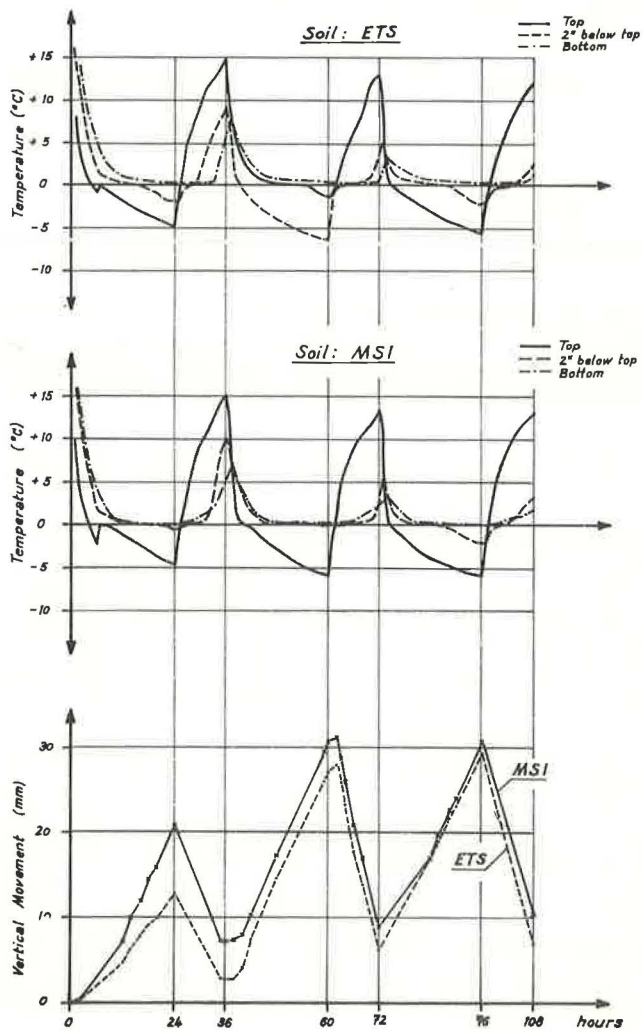

soils can cause frost heaves and detrimental consequences to the pavement and traffic. It is to be noted, however, that the correlation between the instability (alteration of soil structure due to frost action) and the bearing capacity after thawing is not yet known.

Klengel (1) has proposed to characterize the frost effects of soils not only by the frost heave but also by the consistency index [defined as $(w_e - w)/I_p$] of the frozen and thawed soil. The index indirectly gives an indication of the bearing capacity of fine-grained soils. The method is, however, not applicable for the important group of dirty sands and gravels.

The greatest drawback in the case of heave-rate criteria lies in the reproducibility of results. It is indeed a difficult task to prepare samples having water content and density the same as those existing in the field. Relatively small differences of water content can be responsible for different heave rates and soil structure (14). In addition, as a result of unavoidable inhomogeneities in the sample and slight inconsistencies of frost-chamber temperatures, the heave-time relation may lead to curved lines so that a constant heave rate cannot be determined (Fig. 3, 15).

PHASE-INTERFACE CRITERIA

The fundamental investigations on the soil behavior during frost action comprise the thermodynamic equilibrium at the water-ice and water-air interface in connection with the pore diameter. Everett (16) considers the growth of a small crystal immersed in and in equilibrium with a fluid. The difference between the pressure of the solid crystal p_s and the pressure of the liquid p_l is proportional to the surface tension σ and conversely proportional to the crystal radius r.

$$p_s - p_l = \Delta p = \frac{2 \cdot \sigma_{sl}}{r}$$

Hoekstra, Chamberlain, and Frate (17) interpret the pressure difference Δp to be the frost-heaving pressure compared to an atmospheric soil-water pressure. According to their findings, every soil characterized by its pore structure and an effective pore radius r is associated with a certain maximum frost-heaving pressure. A comparison of that maximum frost-heaving pressure with the soil-water tension and the particle content smaller than 0.02 mm shows that the soil-water tension determined by the pore structure is more reliable in predicting frost susceptibility than a single point of the grain-size distribution.

That way, the maximum frost-heaving pressure could be chosen to classify frost susceptibility. Table 3 gives a few test results. (Because not enough data are available, it may be assumed that Augrey sand and Hanover silty sand, having approximately similar gradation curves, will behave in a similar manner when subjected to frost temperatures.) Although frost-heave rates and maximum frost-heave pressures for both the soils are about the same, a vast difference exists in the values of CBR after thaw.

The drawback in using the maximum frost-heaving pressure is that, although 2 soils may be frost susceptible to the same degree, it is possible that the pavement performance of one soil may be satisfactory while that of the other may be entirely unsatisfactory. The reason is that the criteria give no information about the bearing capacity after thaw.

Following another line of thought, Williams (18) compared the penetration of ice surface into the soil pores with the intrusion of air into the pores of the same soil system. He measured the air-intrusion value into the unfrozen sample and, by using the ratio of surface tension ice-water to surface tension air-water, he calculated "ice-penetration value." That value is governed not by the largest pore space but by the largest continuing pore diameter. In the application of that method to road design, the surcharge load on the soil layer and the soil-moisture tension are compared with the ice-penetration value: No frost susceptibility exists if the surcharge load and the pore-water tension exceed the ice-penetration value. Although his method has merit in that

Figure 2. Grain-size distribution of soils.

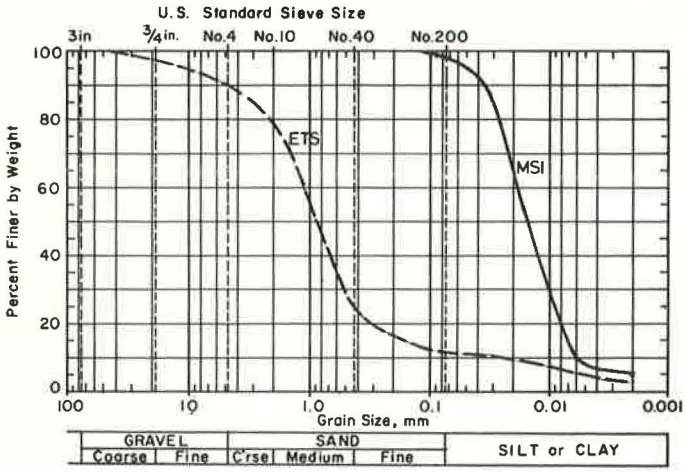

Figure 3. Frost heave of clay-sand mixtures.

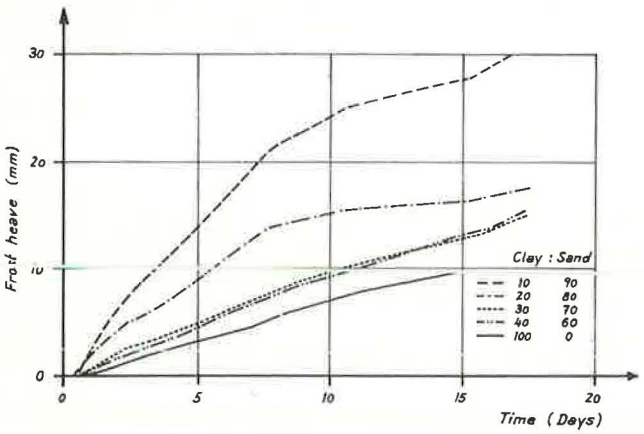

Table 3. Frost-heave rate and maximum frost-heave pressure for sands.

Soil	Frost-Heave Rate (9) (mm/day)	Maximum Frost-Heave Pressure (kp/cm²)	CBR After Thaw (17) (percent)	Particle Content <0.02 mm (percent)	Uniformity Coefficient d_{60}/d_{10}
1 Dirty sand					
AS	—	1.3	—	9	8
HSS	19	—	7.3	7	6
2 Dirty gravelly sand					
HPG	21	1.6	31.7	5.5	29
(2 - 1)/1	0.1	0.19	3.3	-0.31	3.1

it is to be applied to the calculation of the total design thickness, it has the following weaknesses:

1. The data of the example given (18) are not convincing;
2. There is no relation to the actual freezing temperature and the duration of the frost period;
3. The method seems to be unsuitable for dirty sands and dirty gravels; and
4. No information is given as to the remaining bearing capacity after thawing.

SUMMARY

The frost-susceptibility criteria in use can be divided into 3 groups: (a) particle size, (b) frost heave rate, and (c) phase interface.

To meet the practical requirements requires that frost susceptibility be correlated to the bearing capacity of thawed soil. The influence of the freezing process and other external conditions on the bearing capacity of thawed soils ought to be examined.

The survey shows that the term "frost susceptibility" does not fully meet the demands expected of a criterion. It is unfortunate that such a term has taken root in the literature. The term is as vague as that of "slide susceptibility" applied to embankment soils. Although the latter term gives a qualitative picture of the soil, the safety of the embankment can be ascertained only when the stability analysis is made.

It is time that the frost-susceptibility problem be similarly treated as an engineering problem demanding full analyses in terms of the type of soil and the stresses imposed on it by all factors connected with the frost action.

ACKNOWLEDGMENT

Help rendered by Dr. Maini in editing and formulating the paper in English is gratefully acknowledged.

REFERENCES

1. Klengel, K. J. Frost und Baugrund. VEB Verlag für Bauwesen, Berlin, 1968.
2. Richtlinien für die Verhütung von Frostschäden in Strassen. FG Köln Arbeitsgruppe Untergrund, 1968, 12 S.
3. Pavement Design for Frost Conditions. U.S. Army Corps of Engineers, Tech. Manual 5-818-2, 1965.
4. Haley, J. F. Frost Considerations in Highway Pavement Design: Eastern United States. Highw. Res. Rec. 33, 1963, pp. 1-5.
5. Schaible, L. Frost- und Tauschäden an Verkehrswegen und deren Bekämpfung. Ernst und Sohn, Berlin, 1957, 176 S.
6. Kögler, A., Scheidig, H., and Leussink, H. Beitrag zur Frostfrage im Strassenbau. Schriftenreihe Strasse 3, 1936, S. 32-41.
7. Verhütung von Frost- und Tragfähigkeitsschäden an Strassen. Versuchs- und Entwicklungsstelle des Strassenwesen, Ministerium für Verkehrswesen, Berlin Ost, TGL 9942, April 1967, 10 S.
8. Pavement Design and Construction Manual: Section 1—Design and Evaluation of Flexible and Rigid Pavements. Canada Dept. of Transport, Ottawa, 1963.
9. Jessberger, H. L., and Carbee, D. Influence of Frost Action on the Bearing Capacity of Soils. Highw. Res. Rec. 304, 1970, pp. 14-25.
10. Higashi, A. Experimental Study of Frost Heaving. Road Abstr., Vol. 26, No. 10, 1959, p. 221; Highw. Res. Abstr., Vol. 30, No. 2, 1960, p. 25; USA SIPRE, Res. Rept. 45, 1958.
11. Freden, S. The Mechanism of Frost Heave and Its Relation to Heat Flow. Proc., 6th Int. Conf. on Soil Mech. and Found. Eng., 1966, pp. 41, 45; Nat. Road Res. Inst., Stockholm, Spec. Rept. 22, 1964.
12. Croney, D., and Jacobs, J. C. The Frost Susceptibility of Soils and Road Materials. Gt. Brit. Road Res. Lab., Rept. LR90, 1967, 68 pp.
13. Balduzzi, F. Bodenmechanik für den Strassenbau. ETH, Zürich.

14. Springenschmid, R. Der Einfluss des Einbauwassergehaltes auf das Frostverhalten verdichteter und stabilisierter bindiger Böden. Felsmech. u. Ing. Geol., B. 3, H. 3-4, 1965, S. 114-121.
15. Jessberger, H. L., and Zenk, H. Untersuchungen des Bodenfrostes an Tonen und Ton-Sand-Gemischen. Strasse u. Autobahn, B. 14, H. 5, 1963, S. 170-176.
16. Everett, D. H. The Thermodynamics of Frost Damage to Porous Solids. Trans. Far. Soc., Vol. 57, No. 5, 1961, pp. 1541-1551.
17. Hoekstra, P., Chamberlain, E., and Frate, A. Frost Heaving Pressures. Highw. Res. Rec. 101, 1965, pp. 28-38; USACRREL Res. Rept. 176.
18. Williams, P. J. The Nature of Freezing Soil and Its Field Behavior. Norges Geotekn. Inst., Publ. 72, 1967, S. 91-119.

INDIANA'S THERMALLY INSULATED TEST ROAD

James A. Horton, M. M. Bowers, and C. W. Lovell, Jr.,
Joint Highway Research Project, Purdue University

Data presented show that small thicknesses of foam plastic insulation prevented frost penetration into a highway subgrade in an area where the freezing index is less than 1,000 deg days. The data were obtained from a test road (flexible pavement) that was built in northern Indiana and consisted of a control (normal) section with no insulation, a normal section with 1 in. of insulation, and a normal section with the 6-in. subbase eliminated and 1½ in. of insulation added. In the analysis of the 5-variable subsurface temperature problem, 3 of the 4 independent variables—3-dimensional subspace and time—were held constant while the effect on temperature of the fourth was examined. In addition, limited data on differential surface icing of adjacent insulated and uninsulated sections indicate that insulated pavements are colder during a seasonal cooling and uninsulated pavements are colder during a seasonal warming. The overall performance of the insulated sections is satisfactory after 3 winters of service.

•FOAM PLASTIC has become an effective means of preventing frost penetration into a highway subgrade. A number of installations (1) have been built in various northern states of the United Stated and in Canada where winters are very severe. In 1969, the effects of subgrade insulation in a more moderate climate were studied in an insulated test road that was built in north-central Indiana, where the freezing index is generally less than 1,000 deg days. The road was instrumented, and 2 years of data have been collected. This paper summarizes the performance of the road.

LOCATION AND DESIGN

The test installation is on Ind-26, approximately 13 miles east of Lafayette and just west of the Rossville town limits.

A finite difference solution of the 2-dimensional heat flow model developed at Purdue (3) was used in the design of the test installation. That method of design allowed possible design combinations to be easily checked by subjecting them to actual design-year conditions. The design year was the 1962-63 winter, the coldest of the preceding 10 winters, having a freezing index of 1,274 deg days.

Plan and profile views of the test sections are shown in Figure 1 and Figure 2 respectively. Section C is the normal (control) design section. Section A is the same as section C except for a 1-in. thick, 34-ft wide layer of insulation placed on the subgrade surface. The subbase was eliminated in section B, and a 1.5-in. thick, 46-ft wide layer of insulation was placed directly beneath the base course. The temperature sensors, thermistors, were located at the center of each 2,000-ft long section. The thermistors were installed only in the north half of the highway. Figures 3, 4, and 5 show the thermistor positions in sections A, B, and C respectively.

SITE CONDITIONS

Soil borings were located on the northern half of the highway at stations where the thermistors were placed. Also, soil samples were obtained at the time of thermistor

Sponsored by Committee on Frost Action.

Figure 1. Plan of test road.

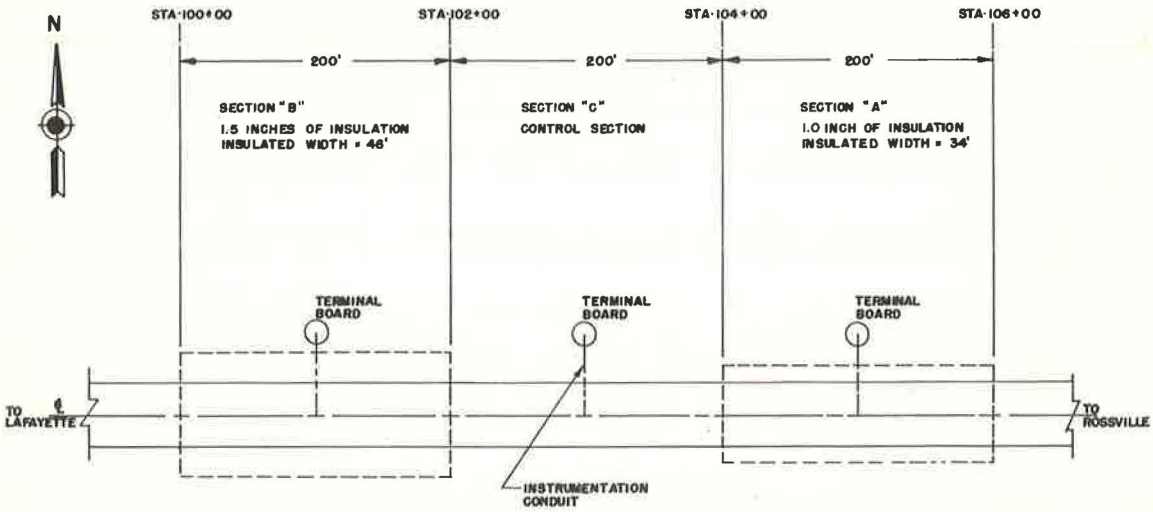

Figure 2. Profile of test road.

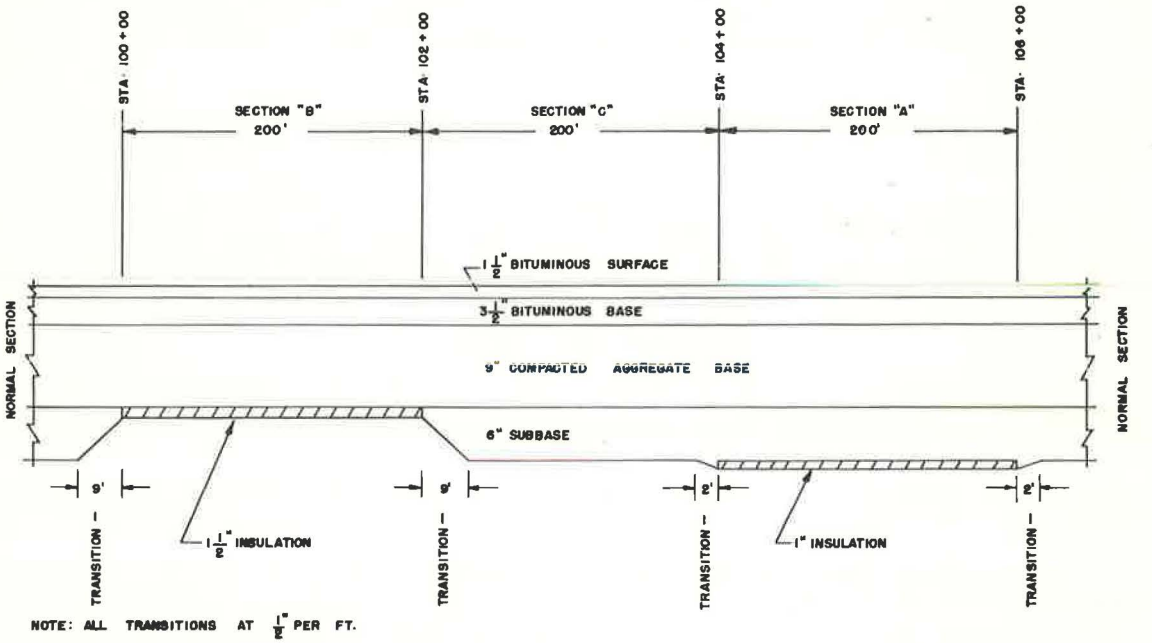

Figure 3. Section A instrumentation.

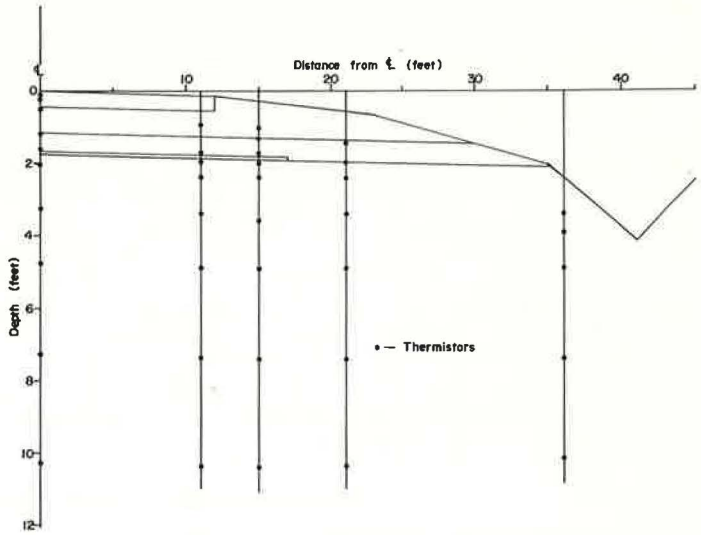

Figure 4. Section B instrumentation.

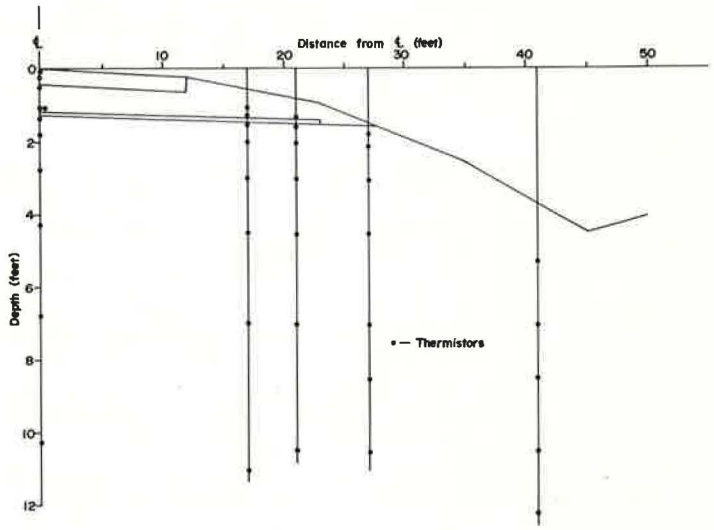

Figure 5. Section C instrumentation.

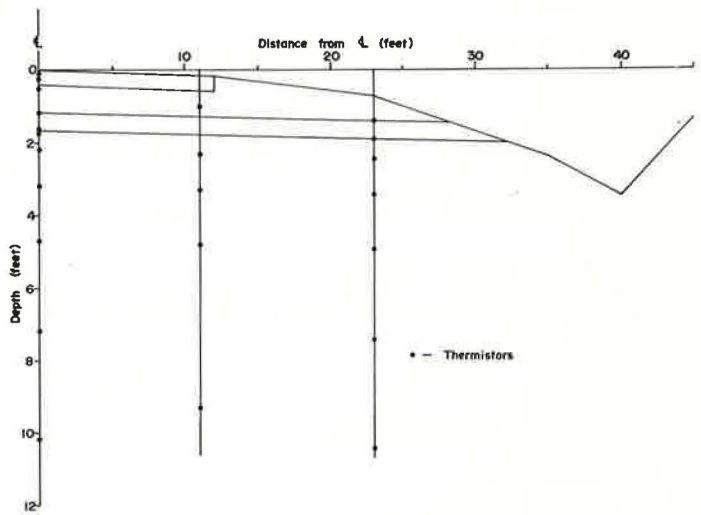

installation from the sides of the 4-ft deep installation trench. From those investigations, the soil profile and moisture conditions were determined.

The subgrade soils of section A are 4 ft of AASHO classification A-2-4 soil over more than 8 ft of A-1-b soil. The water contents of the soils were about 5 to 6 percent. The water table in section A was about 14 ft below the pavement surface. The borings in section A were the only borings in which the water table was encountered. The borings in each section were 11 to 15 ft deep. Section b soils consist of 1 ft of A-2-4 soil over 3.5 ft of A-4 soil over A-6 soil. The water contents were 5, 13, and 17 percent respectively. Section C soils generally consist of 1.5 ft of A-2-4 soil over A-1-b soil. An additional layer of A-1-a soil about 6 in. thick is located 2 ft below the top of the subgrade. Section C water contents were from 5 to 7 percent.

The site was in an area of generally silty soils and was placed in a cut rather than a fill to increase the wetness. Unfortunately, neither soil nor water conditions were such to produce hoped-for high-frost-damage potential. In spite of that, nearly all of the objectives of the study were realized.

PERFORMANCE EVALUATION

Personnel of the Indiana State Highway Commission Research and Training Center collected data at the test installation during the 1969-70 and 1971-72 winters. First-year data were collected every working day. When we found that lesser amounts of data could adequately define the trends, we collected 1971-72 data twice a week except when sudden or extreme periods of cold dictated that additional data were required. The freezing indexes of the 1969-70 and 1971-72 winters were low: 673 deg days during a freezing season of 65 days and 355 deg days during a freezing season of 52 days respectively.

The analysis of subsurface thermal patterns is a 5-variable problem. Temperature is the dependent variable with time and with the 3-dimensional subsurface space. The analysis was conducted by holding 3 of the independent variables constant and studying the effect on temperature of the fourth.

Figures 6 and 7 show a comparison of temperatures at points below the insulation in sections A and B with temperatures at points at approximately the same depth in section C. The effect of the insulation is clearly shown in Figure 6. Section B, having the thicker insulation, remains the warmest of the 3 sections throughout the freezing season. However, care must be exercised when the sections shown in Figure 7 are compared. The combined effect of different thicknesses of insulation and different depths of points makes direct comparison difficult. Comparison of different depths was dictated by the loss of some instrumentation during the 3 years of service. If it is assumed that there is a vertical thermal gradient, i.e., no temperature change, from the depth of the point observed in section B to the same depth as observed in section C, then section B subgrade is warmer. The effect of the insulation is also shown in Figure 8, where the temperature above and below the insulation in section A is compared. The 1-in. insulation was enough to allow the subgrade to remain unfrozen while the temperature directly above the insulation was as low as 17 F.

Figures 9, 10, and 11 show isotherms for each of the 3 sections for January 20, 1970, approximately the time of maximum frost penetration in the control section during the 1969-70 winter. For the uninsulated section, the isotherms are approximately parallel to the ground surface, which is intuitively expected when there is slight lateral variation of soil properties and no snow cover. In sections A and B, the insulation modified both the shape and the magnitude of the isotherm at a given depth. The effect is greater for section B.

Temperature gradients (temperature versus depth curves) are shown in Figure 12 for January 22, 1970. Section B, besides having the warmest subgrade temperatures, has the coldest pavement temperatures. This effect will be discussed in more detail later in the paper.

The depth of penetration of the 32-deg isotherm in section C for the 1969-70 freezing season is shown in Figure 13. Although the penetration was to a depth of 4 ft in section C, the 32-deg isotherm did not penetrate the insulation in either section A or section B.

Figure 6. Temperatures below insulation from Nov. 1969 to March 1970.

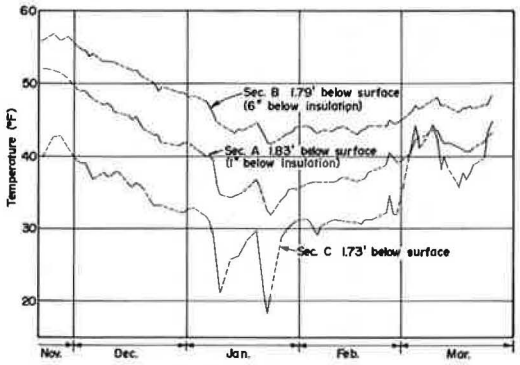

Figure 7. Temperatures below insulation from Nov. 1971 to March 1972.

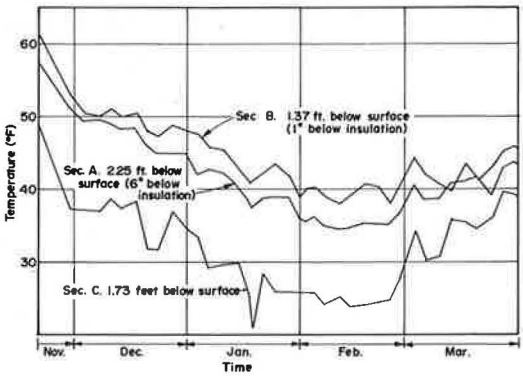

Figure 8. Temperatures above and below insulation from Nov. 1971 to March 1972.

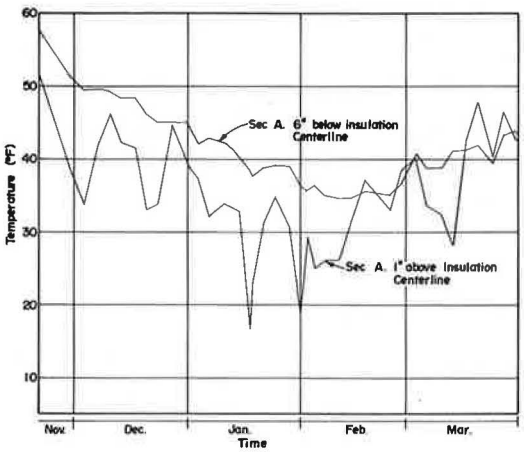

Figure 9. Section A isotherms for Jan. 20, 1970.

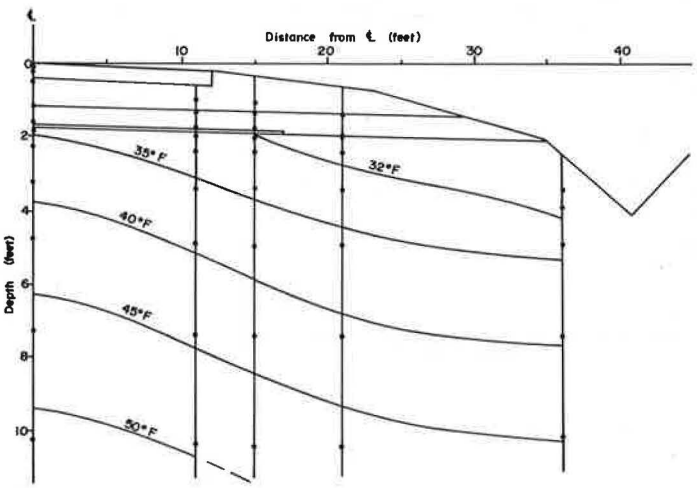

Figure 10. Section B isotherms for Jan. 20, 1970.

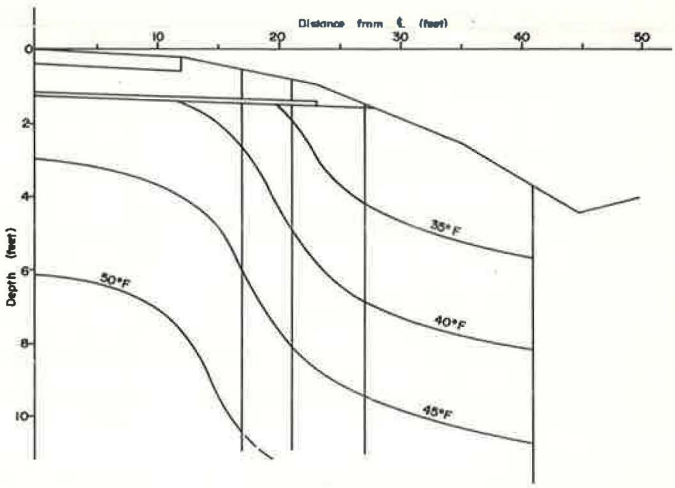

Figure 11. Section C isotherms for Jan. 20, 1970.

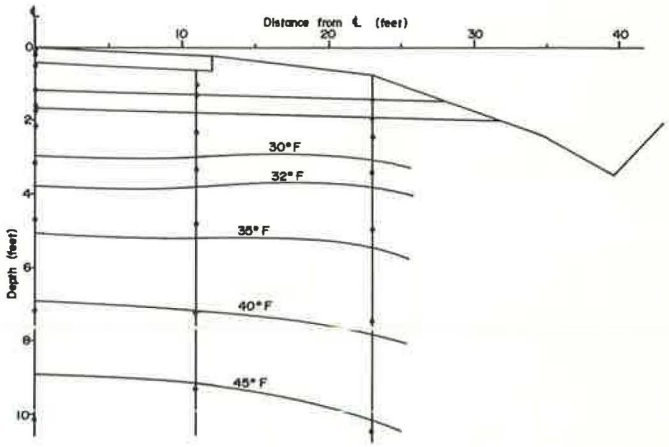

Figure 12. Centerline temperature gradients for Jan. 22, 1970.

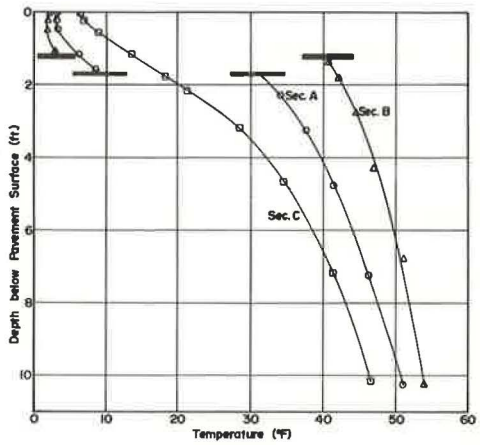

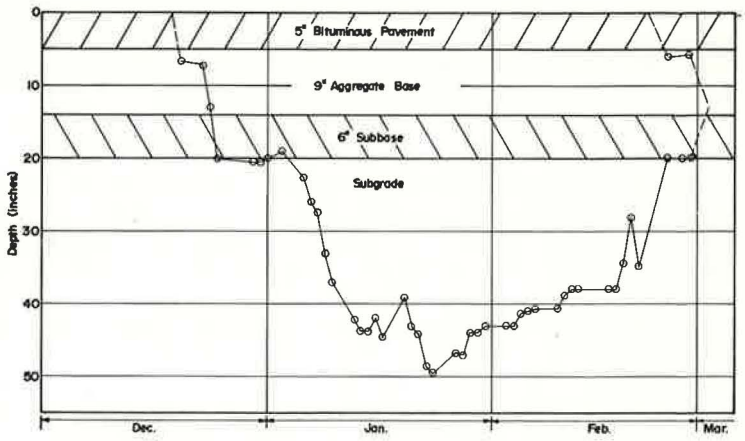

Figure 13. Penetration of 32-deg isotherm into uninsulated section during 1969-70 winter.

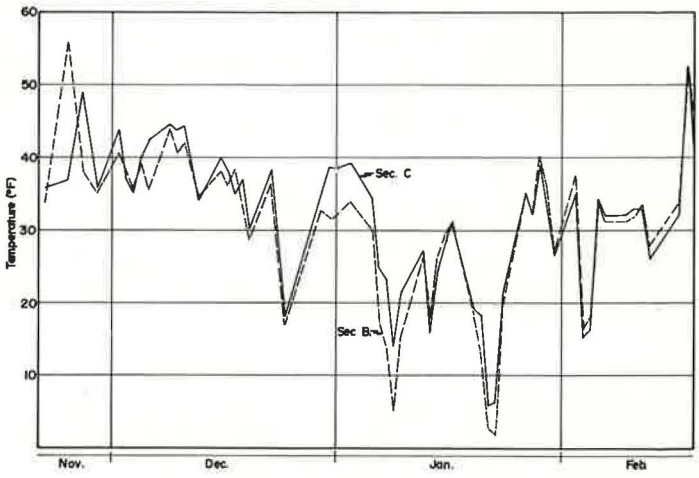

Figure 14. Temperature 1 in. below pavement surface from Nov. 1969 to Feb. 1970.

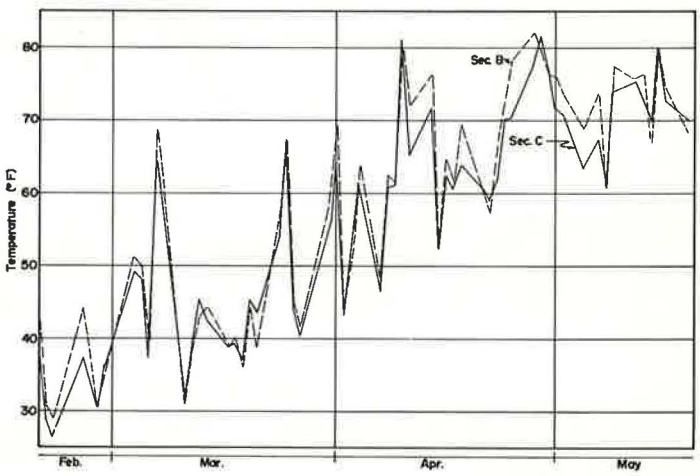

Figure 15. Temperature 1 in. below pavement surface from Feb. to May 1970.

Some transverse and longitudinal cracking of the bituminous surface has developed on the test sections, but the cracking is consistent with cracking that has occurred outside the limits of the test site. Thus, it does not seem likely that the insulation has lead to any poor structural performance.

ICING POTENTIAL STUDY

The presence of an insulation layer will alter the normal heat flow through a pavement. Subgrade insulation used in sections of limited length can produce different temperatures in adjacent insulated and uninsulated pavement surfaces and cause preferential icing of those surfaces. Figures 14 and 15 show the temperatures of points 1 in. below the pavement surfaces in sections B and C for 1969-70. The general trend is that pavement above the insulation may be either cooler or warmer than the adjacent pavement without insulation, depending on whether the air temperature is in a general cooling trend or a general warming trend.

An attempt was made to observe whether any degree of differential icing occurred on the test road during the 1971-72 winter. The distance of the test installation from Purdue University limited that study to a random daily observation of the pavement condition. No differential icing was observed during the survey, but some difference in behavior was observed. On a number of occasions, the insulated sections were darker in color because of the presence of moisture in the minute surface cracks of the asphaltic surface. The reverse situation was also seen when, during a light snowfall, the insulated sections remained dry because the snow was blown off the colder surface but melted on the warmer uninsulated section and caused the pavement surface to be slick.

The findings of this study with respect to differential pavement icing are inconclusive for several obvious reasons. However, generally the tendency for an insulated section to ice with respect to an uninsulated one (or vice versa) depends on the general trend of air temperatures (Figs. 14 and 15). The insulated sections are more likely to have surface ice during a general cooling trend, and the uninsulated sections are more likely to have ice during a general warming trend.

CONCLUSIONS

Data show that samll thicknesses of insulation—1 and 1.5 in.—were sufficient to prevent subgrade frost penetration in areas of low freezing indexes.

Although no surface icing was encountered during the study, the conclusion that icing is not a problem is inadvisable because of the limited number of pavement observations. In general, the insulated sections are more likely to ice during seasonal cooling, but the uninsulated ones are more likely to ice during seasonal warming.

The 2-dimensional heat flow model is an effective thermal design tool in that combinations of thickness of insulation and depth of placement may be compared with relative ease and for each the appropriate combination can be selected for the specific design situation.

ACKNOWLEDGMENTS

The authors wish to thank the personnel of the Indiana State Highway Commission Research and Training Center for the collection and reduction of data. Appreciation is also expressed to the Joint Highway Research Project, a cooperative effort of Purdue University and the Indiana State Highway Commission, for financial assistance during the study.

REFERENCES

1. Performance Study Report on Insulation Board (Polystyrene). AASHO-ARBA Subcommittee on the Development, Evaluation and Recommendation of Hew Highway Materials, 1970.
2. Bowers, M. M. Thermally Insulated Test Road: State Road 26—Performance and Temperature Prediction Studies. Purdue Univ., Lafayette, Ind., Joint Highw. Res. Proj. Rept. 2, March 1972.

3. Ho, D. M. Prediction of Frost Penetration Into a Soil-Water System. Purdue Univ., Lafayette, Ind., PhD thesis, Aug. 1969.
4. Horton, J. A. Thermally Insulated Test Road: State Road 26—Final Performance and Temperature Prediction Studies. Purdue Univ., Lafayette, Ind., Joint Highw. Res. Proj. Rept. 39, Nov. 1972.
5. Stulgis, R. P. Insulated Test Road: State Road 26. Purdue Univ., Lafayette, Ind., Joint Highw. Res. Proj. Rept. 12, July 1968.
6. Toenniessen, J. D. Thermally Insulated Test Road: State Road 26—Phase II, Performance Studies. Purdue Univ., Lafayette, Ind., Joint Highw. Res. Proj. Rept. 10, May 1970.

TEMPERATURE INSTRUMENTATION FOR INDIANA'S THERMALLY INSULATED TEST ROAD

H. R. J. Walsh, Research and Training Center, Indiana State Highway Commission

Three thermally insulated test sections were built into an Indiana highway as part of an improvement project. The data collection system included 105 temperature transducers of the thermistor type buried within the test sections. Information is provided principally on the selection, fabrication, installation, and operation of the transducers, which were found to be reliable and economical.

•THE INDIANA thermal test road consisted of 3 instrumented test sections built into an active highway. Each test section was 200 ft long and differed from one another in the amount of foam plastic insulation installed at the top of the subgrade and in total depth of the pavement. The test road and data obtained from it are described in other reports (1, 2, 3, 4, 5, 6).

This paper presents information on the temperature instrumentation system used. The problem is described, and details are given on the instrument fabrication and field installation and on the data acquisition method. Information is also provided on the calibration procedure and on the precision and durability of the instruments.

NATURE OF THE PROBLEM

The innovations in the temperature-measuring system used on this project were the result of the need to meet a limited time schedule within existing budgetary and administrative restrictions. Frost effects are not so severe and widespread a problem in Indiana as in some other areas and are more easily handled because of Indiana's climate and soil conditions. However, the corrective action is often expensive and depletes the available aggregates. Therefore, the proposal by Purdue University to initiate studies of the use of foam-plastic insulation to reduce those costs was encouraged. A time schedule was adopted that was viewed likely to create some difficulties but to maintain the interest of the faculty and graduate students at Purdue and meet their academic schedules and requirements. Meeting the time schedule was a problem for the Research and Training Center, a new organization within the State Highway Commission. The center had little experience in this specific area of work or equipment applicable to it and had an overriding need to devote its limited budget for equipment purchases to items that could be of general utility for a variety of projects.

Instruments available on the market were of the thermocouple type. They are self-generating transducers that produce an electromotive force proportional to a temperature change. A sensitive and precise galvanometer or potentiometer is used to convert that force into temperature. Those instruments would be hard to adapt for use on other projects where the measurements would involve transducers operating on different principles. Furthermore, it is necessary each time readings are taken to have reference points in the circuit at a selected temperature. Inasmuch as readings were to be taken only once each day over a period of some months, an installation in which the reference points could be held at the selected temperature and continuous recorders protected was not justifiable.

Sponsored by Committee on Frost Action.

It was eventually decided that some form of thermistor would be used. Thermistors had been used in temperature measurement in a number of cases, although none had been buried in earth materials. The thermistor is a semiconductor, crystal, electronic element that undergoes a change in resistance when its temperature changes. It is commonly used in television sets as a means of limiting current to a safe level until the unit warms up to operating temperatures. It has also been used in temperature-measuring instruments. Selecting the thermistor simplified the data acquisition apparatus enormously because only a resistance-measuring device, such as an ohmmeter, would be needed. Such instruments were available in portable battery-operated form suitable for field use and required no reference temperature source. Thermistors were also capable of the required precision in temperature measurement because their resistance is calculated from an expression in which temperature is in the exponent, and many change resistance by a factor of 10 for a small temperature change. Thus, the problem of burying them in soil was the only remaining one.

SITE CONDITIONS

A part of the urgency to provide instrumentation resulted from the fact that a highway improvement project was scheduled in an area having frost-susceptible soils, and the test road was to be installed as part of that project. The location of the test installation was at the west edge of the city of Rossville where electric power was available for operating the electronic recording systems. A long cut was to be made with adequate length for the three 200-ft test sections, all of which would have a uniform grade and drainage condition, including deep side ditches and wide shoulders cut in the undisturbed soil. The soils at the site were principally silty sands, with sand fractions ranging from fine to coarse but predominately fine and in excess of 35 percent of nonplastic fines.

The contract provided for the placement of the foam-plastic insulation board by the contractor, for the various changes in subbase depth and in elevation of the finished subgrade at the test sections (including deletion of undercutting, which is normal in frost-susceptible soils), and for a limited amount of trenching by the contractor at the middle station of each of the test sections for installation of gauges. The length of time that the trenches were to be left open was limited, and state employees were to install the instruments in them and to do so with minimum interference with the contractor's overall operation. A total of 105 temperature measuring transducers were installed (an equal number in each test section) at locations ranging from the centerline of the roadway to the ditch on the north side and at depths as great as 14 ft below the surface of the finished pavement.

TRANSDUCER FABRICATION

The transducers selected were small glass-encapsulated thermistors in the shape of a bead (Fenwall Electronics, Inc., model EA33JM8). Figure 1 shows one of those beads in an early stage of transducer fabrication. When received from the manufacturer, each bead is approximately $^1/_{10}$ in. in diameter, and has 2 bare-wire leads approximately $^1/_{100}$ in. in diameter. The thermistor shown in Figure 1 already has a short length of hookup wire attached to each of the leads. The hookup wire permits the first soldering operation to occur without the heat damaging the thermistor itself, even with the little heat sink provision possible at that state. Also it increased the durability of the assembly during work in the next stages and made it easier to heat sink during the later soldering to the full length of lead cable.

The complete assembly is shown in Figure 2. In the second step, a length of heat-shrink insulation tubing was slipped over each of the lead assemblies developed (Fig. 1) and shrunk in place over the solder connection between the hookup wire and the thermistor lead. Then the ends of the hookup wires were stripped, connected, and soldered to the stripped ends of a 2-conductor polyvinyl-chloride (PVC) sheathed cable. A single length of vinyl electrical tape was then wrapped lengthwise about each lead from the shrunk tubing to the insulation on the conductor of the cable. That with the shrunk tubing provided a positive separation and prevented shorts between the leads. Two turns

of tape were placed around the end of the sheath of the 2-conductor cable to protect it from being cut, and a wrapping of wire was installed and tightly twisted over the taped sheath to prevent water infiltration and to provide a mechanical connection between the sheathed cable and the epoxy encapsulation.

Finally, the entire transducer assembly was encapsulated in a commercial epoxy that contained no volatile material (Fig. 3). Thus, 100 percent of the weight of material used in the mixture reacted and remained as part of the completed epoxy casting, and no water holes or porosity developed by evaporation of the solvents. A block of paraffin served as a mold for the casting. Grooves having a minimum width and depth slightly greater than ½ in. and a pointed tip at each end were cut in it with a hot iron. The transducer assembly was suspended in the middle of the space so provided and held in place by melting and clamping wax around the 2-conductor lead cable. The groove was long enough to contain the entire transducer assembly and the twisted sealing wire tires. This casting process was possible because the wax did not mix with the liquid epoxy, interfere with its reaction, or adhere to it strongly.

The epoxy was mixed and poured slowly into each of the grooves to fill it completely to the top and was then allowed to set for a minimum of 4 days. The completed transducer, after being removed from the mold, could be visually inspected for defects in casting or location of transducer elements within the epoxy mass because the material remained reasonably transparent. The transducers were cured in an oven at approximately 125 F for 24 hours (according to manufacturer's recommendations, the thermistors were not to be exposed to temperatures higher than 150 F because of a possibility of altering their electrical characteristic). Finally, the transducers were left in a bath of saltwater for a few days and then checked for resistance and for shorts between conductors or from the conductors to the solution. Of the 115 transducers constructed, only 3 had defects, and the 105 selected for actual field use were those that were the most similar in resistance at a series of known temperatures compared to the calibration curve provided by the thermistor manufacturer.

ASSEMBLY FOR FIELD INSTALLATION

So that their field installation would cause no delay to the contractor, the temperature transducers were assembled in the laboratory into a final wiring harness that was ready for burial without further connection work. That also permitted laboratory waterproofing and testing of any splices to be buried and made it possible to reduce the number of long cables to be handled in the field because the wires to a group of transducers that would be buried close to each other could be joined into single multiconductor cables. Eight-conductor cables with PVC sheathing were used as the multiple-circuit cables. The connection to the 8-conductor cable was planned to be located at a point convenient to each of the transducers to be connected to it, and the length of the 2-conductor cable attached to each transducer during its fabrication had been chosen to provide that length plus at least 2 ft of slack. Each of the 8-conductor cables was cut to a length slightly longer than needed to stretch from that connection point to a point on the shoulder slope of the completed highway where eventually a junction box would be located, in which temperature readings for that test section would be obtained.

Each of the 2-conductor cables was tagged according to its position when the transducer was finally installed in the grade, and then all in that group were connected to the 8-conductor cable at a single point. In that connection, 2 of the conductors in the 8-conductor cable were connected in common to one of the leads from each of the transducers involved in that part of the test section. As many as 6 transducers, each having a single color-coded conductor within the 8-conductor cable, were connected to the 8-conductor cable to a junction box to be used in the final field installation.

A junction box with the 8-conductor cable connected to it is shown in Figure 4. Each of the 8-conductor cables was led in, tied down, and connected to an 8-connector terminal strip, labeled and marked in such a manner that the resistance of each transducer could be read between a common terminal and one of the other connecting points, at which the transducer could be identified. The boxes used were metal military ration boxes, which have a waterproof metal lid and inside dimensions of approximately 12 x 12 x 15 in.

FINAL CALIBRATION

The thermistors were all of a single lot and were checked by the manufacturer to ensure that each had a certain calibration value within a very narrow tolerance range. This tolerance range, of course, was much closer than would be required for the eventual field use, but it might have been altered somewhat by the heating and handling in fabrication as well as by the characteristics of the lead wires. Therefore, the final calibration was checked. When the individual transducers had been tested and found free from shorts, those fitting the calibration curve most closely were selected for use in the field installation. Each of those fit a single calibration curve well enough that no reading at any temperature within the expected range would vary from the expected value within more than $^1/_{10}$ of 1 F.

Figure 5 shows the entire set of assembled transducers, complete with junction boxes, during the final calibration process in the laboratory. All of the transducers were immersed in a standard laboratory-temperature bath containing saltwater and then wrapped in fiber-glass insulation. Adding ice or setting the temperature control brought the water bath to a chosen temperature at 10 deg intervals between 0 and 150 deg where it was allowed to stabilize before readings were taken. The resistance of each gauge was read, and a check was made for shorts between leads and the water in the bath. All but 2 transducers as finally assembled met the manufacturer's calibration curve with an accuracy of less than $^1/_{10}$ of 1 F at each temperature. The other 2 transducers were fully operational except for slight shifts in their calibrated values, probably from a resistance difference in some point within the cabling, and special calibration curves were made for use in interpreting their results. No transducers were found to be defective or to have failed during that process, and the assembly was then ready for field use.

Figure 5 also shows the means of connecting the 8-conductor cable and the 2-conductor cables used for each of the transducers. That connection was fully encapsulated in cast epoxy in the same general manner as each of the transducers had been. Before the calibration procedure was begun, those encapsulated connections had also been soaked in a saltwater bath and checked for shorts or other evidence of water penetration.

FIELD INSTALLATION

At each of the test sections, installation of transducers began after the grading operation had cut the subgrade to its finished elevation. At that point, the contractor dug a trench 6 ft deep from the centerline of the roadway to the break of the shoulder. The transducer assemblies were then brought to each of the test sections. Only those transducers and cables could be installed that would be below the foam-plastic insulation or the top of the finished subgrade and in the width that would be beneath the pavement itself or the shoulder. The location of each transducer was established by taping from the centerline and shooting with a level to find its final position. The transducers installed below the bottom of the trench were suspended into holes drilled below the bottom of the trench with an auger. Figure 6 shows transducers during the process of installation when backfilling of the trench itself was nearly complete, and Figure 7 shows the tangle of conductors that might be expected to develop during the process of laying and sorting that many cables. Although the process appears to be confusing, the tagging method and record-keeping process were such that this was actually as organized as many construction operations. As a final check, each transducer was electrically identified at the time of installation by an electronic meter across its terminals in the junction box while being warmed by hand to produce a resistance change.

A sand used as backfill material was from the project and contained little material passing the No. 200 sieve. It was dried by the contractor in his bituminous plant and was poured by hand into the trench in a thin stream from a few feet above, a method that developed a density well above the minimum. The backfill of the auger holes was done by the same method. In addition, the backfill material in the trench was compacted in layers by standard vibratory equipment as the transducer placement progressed. Those transducers placed above the bottom of the trench were actually installed in a

Figure 1. Thermistor after first step in transducer fabrication.

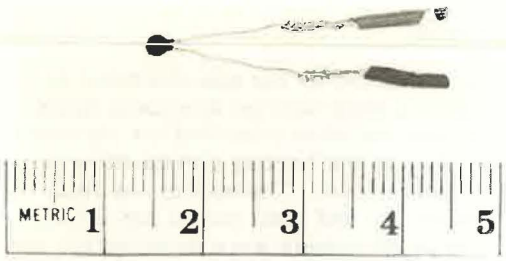

Figure 2. Completed transducer assembly.

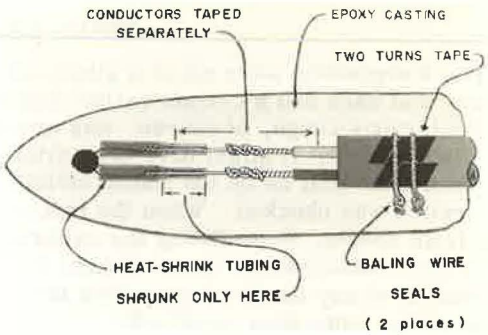

Figure 3. Casting of epoxy envelope.

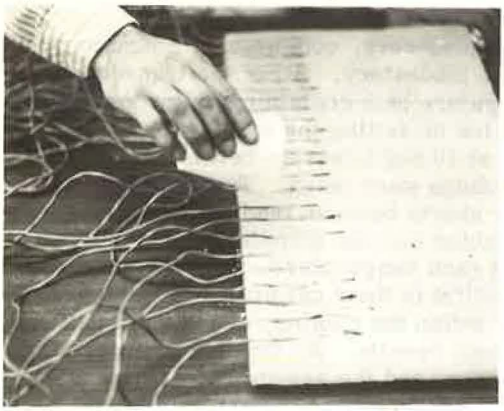

Figure 4. Terminals in junction box.

Figure 5. Calibration of wired system for field installation.

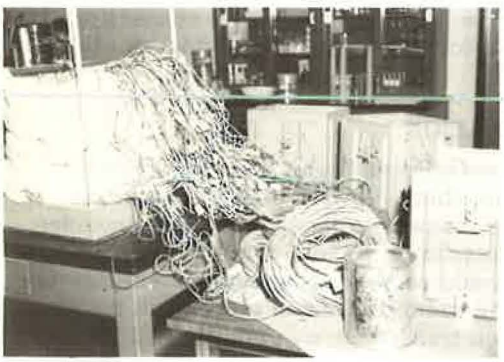

Figure 6. Transducers being buried in shoulder area beneath subbase.

Figure 7. Wired system during placing in shoulder area.

small hole driven into the wall with a sharpened rod. The transducer lead was allowed to hang slack from such a point to the bottom of the trench as backfilling proceeded; enough slack was held at the transducer's location to prevent it from being pulled out by the placement of the backfill.

Field installation of all of the transducers below the finished subgrade surface was completed in fewer than 3 days. At night and after the completion of this stage, the junction boxes and the remaining cables and transducers were loosely buried in the end of the trench. No further placement was done until the foam-plastic material and the subbase layers were all in place. At that time, a trench approximately 4 in. deep was dug by hand in the subbase across from each box to the centerline, and the transducers that were to be within that material were installed. The transducers that were to be installed in the bituminous layers above the subbase were shallowly buried directly beneath their installation points with enough slack wire to permit installation. Those trenches were eventually backfilled by hand with dried and vibrated material. Transducer placement then stopped until the flexible pavement surface was completely in place.

During that interval, the contractor completed ditch grading and sodding. When his work on the pavement surface and ditch was complete, holes were dug in the pavement at the points where the transducers to be in the bituminous pavement had been left. The transducers and their slack wire were recovered from the subbase and put in place, and the holes in the pavement and subbase were backfilled with bituminous mixture, which was obtained hot from the contractor's plant in small quantities and tamped by hand to normal density. Thereafter, the boxes themselves were excavated, the excavation from which they had been removed was enlarged, and a pit was constructed of concrete block and mortar and a steel-plate cover fitted with padlocks to protect the junction box. A small trench was dug by hand out through the ditch slope, and the gauges in that area were installed. As the ditch was filled, a drain was installed from the bottom of the concrete pit to remove any surface water that might enter under its steel cover. The cables, of course, were let in through the bottom of the pit during its construction. The junction box was then placed in the pit, and the cover was installed. When that installation was completed, only 3 transducers had become nonoperational, probably because of breaks in their lead cable during handling or as a result of earth movements during compaction or similar construction operations.

DATA COLLECTION

The portable, battery-operated meter for taking the resistance readings from the transducers (model 300 digital passive scaler manufactured by Western Reserve Electronics) could read all functions to 3 significant digits that were visible on the knobs that were used to adjust to a null balance (Fig. 4). To obtain the readings in a car required the installation of extension cables that could be coiled and left within the junction box such that a board similar to the board in the junction box could be lifted out and taken to a car parked at the location of the concrete pit. That simplified reading and provided more comfort for the technician obtaining the data. A reading was obtained by attaching one lead of the digital scaler to the common point for the transducers connected to a single 8-conductor terminal strip and by touching the other lead to the other terminals of that strip in turn. The readings of resistance were manually recorded by the operator, reduced to temperature by center personnel using calibration curves, and reported to Purdue personnel for their use.

An operator could normally complete the process within 2 hours, including the time to drive the 13 miles or more from the center to the site and back. During that period, he would also obtain the necessary readings from the standard weather station installed in connection with the project and would make other routine observations as required, for example, the depth of water in stand pipes that had been installed along the shoulder line to indicate the water table and of any patterns of ice or snow and their depth on the pavement surface and in the ditch lengths through the test sections. Reduction of the data obtained in a single day into a tabulated form for delivery to the personnel at Purdue usually required less than an hour of time at the center.

RESULTS

The temperature instrumentation system operated well during a 3-year period when data were read daily for the first and last winters and at other times on a less continual schedule. More than 95 percent of the transducers were still yielding data at the end of the first winter, and 85 percent of them were still operating properly and giving accurate data at the end of the third winter. Most of those that were not yielding reasonable data had either open or shorted circuits.

ACKNOWLEDGMENTS

This study was a cooperative effort between Purdue University personnel under the Joint Highway Research Project and personnel of the Indiana State Highway Commission's Research and Training Center. Personnel of the Research and Training Center whose efforts made this a practical project include Nils Johansen, Michael Drudge, William Balensiefer, Charles Yoder, and David Bowman. The center also benefitted from the cooperation and encouragement of the Purdue personnel concerned and the confidence and patience they demonstrated while proceeding with their parts in the program at the time the instrumentation was still being developed.

REFERENCES

1. Horton, J. A., Bowers, M. M., and Lovell, C. W., Jr. Indiana's Thermally Insulated Test Road. Paper presented at the HRB 52nd Annual Meeting and published in this RECORD.
2. Stulgis, R. P. Insulated Test Road: State Road 26. Purdue Univ., Lafayette, Ind., Joint Highw. Res. Proj. Rept. 12, July 1968.
3. Ho, Da-Min. Prediction of Frost Penetration Into a Soil-Water System. Purdue Univ., Lafayette, Ind., PhD thesis, Aug. 1969.
4. Toenniessen, J. D. Thermally Insulated Test Road: State Road 26—Phase II, Performance Studies. Purdue Univ., Lafayette, Ind., Joint Highw. Res. Proj. Rept. 10, May 1970.
5. Bowers, M. M. Thermally Insulated Test Road: State Road 26—Performance and Temperature Prediction Studies. Purdue Univ., Lafayette, Ind., Joint Highw. Res. Proj. Rept. 2, March 1972.
6. Horton, J. A. Thermally Insulated Test Road: State Road 26—Final Performance and Temperature Prediction Studies. Purdue Univ., Lafayette, Ind., Joint Highw. Res. Proj. Rept. 39, Nov. 1972.

SPONSORSHIP OF THIS RECORD

GROUP 2—DESIGN AND CONSTRUCTION OF TRANSPORTATION FACILITIES
John L. Beaton, California Division of Highways, chairman

SOIL AND ROCK PROPERTIES AND GEOLOGY SECTION
L. F. Erickson, Idaho Department of Highways, chairman

Committee on Physicochemical Phenomena in Soils
James K. Mitchell, University of California, Berkeley, chairman
Kandiah Arulanandan, Gerald H. Brandt, Leslie G. Bromwell, Richard W. Christensen, Turgut Demirel, Sidney Diamond, Donald H. Gray, Earl B. Kinter, Joakim G. Laguros, Mo Chih Li, Charles A. Moore, Harold W. Olsen, Robert E. Paaswell, Gilbert L. Roderick, Elmer A. Rosauer, Dwight Abram Sangrey, Mehmet A. Sherif, Hans F. Winterkorn

Committee on Frost Action
Edward Penner, National Research Council of Canada, chairman
Wilbur J. Dunphy, Jr., L. F. Erickson, Hamilton Gray, E. R. Greek, Wilbur M. Haas, Frank B. Hennion, Alfreds R. Jumikis, Chester W. Kaplar, Miles S. Kersten, Clyde N. Laughter, George W. McAlpin, Marvin D. Oosterbaan, R. G. Packard, Harold R. Peyton, C. K. Preus, A. Rutka, Arthur L. Straub, Willis H. Taylor, Jr., Wayne G. Williams

Committee on Environmental Factors Except Frost
William G. Weber, Jr., Pennsylvania Department of Highways, chairman
Richard G. Ahlvin, K. A. Allemeier, Lindo J. Bartelli, Barry J. Dempsey, Wilbur M. Haas, T. Allan Haliburton, Robert D. Krebs, Robert L. Lytton, Leonard T. Norling, J. Frank Redus, Arthur L. Straub, H. C. S. Thom, Thomas H. Thornburn, Edgar Pierron Ulbricht, Larry M. Younkin

John W. Guinnee, Highway Research Board staff

The sponsoring committee is identified by a footnote on the first page of each report.